DEFENCE R&D DÉFENSE

Numerical Simulation of Flows Near and Through a Two-Dimensional Array of Buildings

Eugene Yee
Defence Research Establishment Suffield

Fue-Sang Lien and Yonghua Cheng
University of Waterloo

Defence R&D Canada
Technical Report

DRES TR 2001-115

December 2001

National Defence Défense nationale

Canada

Numerical Simulation of Flows Near and Through a Two-Dimensional Array of Buildings

Eugene Yee
Defence Research Establishment Suffield

Fue-Sang Lien and Yonghua Cheng
University of Waterloo

Defence Research Establishment Suffield

Technical Report

DRES TR 2001-115

December 2001

Author

Eugene Yee

Approved by

C. Boulet

Cam Boulet
H/CBDS

Approved for release by

J. Fitzgerald for

Robert Herring
DRP Chair

Abstract

A numerical simulation has been performed of turbulent flow near and through a two-dimensional array of rectangular buildings (bluff bodies) in a neutrally stratified background flow. The model used for the simulation was the steady-state Reynolds-averaged Navier-Stokes equations with an isotropic, linear eddy viscosity formulation for the Reynolds stresses; and, the eddy viscosity was determined using a high-Reynolds number form of the k-ϵ turbulence-closure model with the boundary conditions at the wall obtained with the wall-function approach. The resulting system of partial differential equations along with the concomitant boundary conditions for the problem was solved using the SIMPLE algorithm in conjunction with a non-orthogonal, colocated, cell-centered, finite volume procedure. The predictive capabilities of the numerical simulation of urban flow are validated against a very detailed and comprehensive wind tunnel data set. Vertical profiles of the mean streamwise and vertical velocities and the turbulence kinetic energy are presented and compared to those measured in the wind tunnel simulation. In addition to the comparison between modeled and measured results, the numerical simulation is used to aid in the interpretation of certain features of the flow observed in the wind tunnel simulation. It is found that the overall performance of the model is good—most of the qualitative features in the disturbed turbulent flow field in and near the building array are correctly reproduced, and the quantitative agreement is also generally fairly good (especially for the mean velocity field). The underestimation of the turbulence energy levels may arise from the inability of the model to capture the subtle effects of secondary strain, especially those associated with curvature, on the turbulence.

This page intentionally left blank

Executive summary

Introduction: It is anticipated that Canadian Forces (CF) in the foreseeable future will have to fight in or protect urban areas, whether in battle, peace-making, peace-keeping, or counter-terrorist operations. The increased awareness and importance accorded by the public worldwide and their governments to maintain appropriate defences against chemical and biological warfare (CBW) agents in an urban (built-up) environment, the prediction of casualties and human performance degradation resulting from such releases, and the development of operational procedures and regulations to control, mitigate, and monitor the fate of CBW agents in urban areas with high population densities, will require mathematical modeling of urban wind flows and dispersion. In this regard, it should be noted that the prediction of urban canopy flow is in principle pre-requisite to or co-requisite with the prediction of scalar (e.g., CBW agent) dispersion within a canopy.

Results: A numerical simulation has been performed of turbulent flow near and through a two-dimensional array of rectangular buildings (bluff bodies) in a neutrally stratified background flow. The model used for the simulation was the steady-state Reynolds-averaged Navier-Stokes equations with an isotropic, linear eddy viscosity formulation for the Reynolds stresses; and, the eddy viscosity was determined using a high-Reynolds number form of the k-ϵ turbulence-closure model with the boundary conditions at the wall obtained with the wall-function approach. The resulting system of partial differential equations along with the concomitant boundary conditions for the problem was solved using the SIMPLE algorithm in conjunction with a non-orthogonal, colocated, cell-centered, finite volume procedure. The predictive capabilities of the numerical simulation of urban flow are validated against a very detailed and comprehensive wind tunnel data set. Vertical profiles of the mean streamwise and vertical velocities and the turbulence kinetic energy are presented and compared to those measured in the wind tunnel simulation. In addition to the comparison between modeled and measured results, the numerical simulation is used to aid in the interpretation of certain features of the flow observed in the wind tunnel simulation. It is found that the overall performance of the model is good—most of the qualitative features in the disturbed turbulent flow field in and near the building array are correctly reproduced, and the quantitative agreement is also generally fairly good (especially for the mean velocity field). The underestimation of the turbulence energy levels may arise from the inability of the model to capture the subtle effects of secondary strain, especially those associated with curvature, on the turbulence.

Significance and Future Plans: The k-ϵ turbulence-closure model with an isotropic, linear eddy viscosity is the simplest complete turbulence model (viz., no advance knowledge

of any property of the turbulence is required for the simulation other than the initial and/or boundary conditions for the problem) that is available currently, and its moderately good predictive performance of the developing flow through an array of two-dimensional buildings without the need to adjust any closure constants is encouraging. This model may be useful as a general-purpose simulator of urban flows since it is simple enough to be tractable numerically and, hence, not require excessive computing time. However, before this model (or, variants of it) can be used for this purpose, it needs to be validated against more experimental data for flow in various obstacle arrays. From this perspective, the availability of extensive and accurate experimental data for flow through various obstacle arrays is urgently required. Finally, the accurate prediction of urban dispersion requires knowledge of the mean wind and turbulence through the urban area. The utility of the urban flow simulation models investigated here for provision of the disturbed wind field statistics required for a physically-based dispersion model needs further investigation.

Yee, E., Lien, F. S., and Cheng, Y. 2001. Numerical Simulation of Flow Near and Through a Two-Dimensional Array of Buildings. DRES TR 2001-115, Defence Research Establishment Suffield.

Table of contents

This page intentionally left blank

List of Figures

Acknowledgements

The authors would like to thank Dr Michael Brown (Los Alamos National Laboratory) for generously providing the wind tunnel data sets for the two-dimensional building array.

Introduction

In recent years, a great effort has been made to understand the impact of large numbers of discrete bluff obstacles (e.g., buildings, trees, and other obstructions within a small domain inside a large city) on the atmospheric boundary-layer flow because of its importance in many aspects of meteorology, wind engineering, and environmental science. In particular, prediction of how the speed, direction, and turbulence of the wind changes as it blows over urban surfaces is in principle pre-requisite to the prediction and understanding of the transport and turbulent diffusion of contaminants within an urban environment. Indeed, in response to increasing concerns on the use of chemical and biological warfare (CBW) agents against military and civilian populations in urban areas, there has been a concerted effort by a number government and military research laboratories and agencies to develop models that can predict the turbulent flow and dispersion in urban areas (e.g., Defense Threat Reduction Agency Urban Dispersion Model Working Group, Department of Energy Chemical and Biological National Security Program).

As far as numerical modeling of urban flows is concerned, most of the effort has been concentrated on modeling the flow around isolated structures or single buildings rather than around groups of obstacles or building clusters. Prognostic models that solve the Reynolds-averaged Navier-Stokes equations have been used to describe the flow field around an isolated cuboid or building (Patterson and Apelt [1]; Zhang et al. [2]; Zhou et al. [3]; Cowan et al. [4]) or the interaction of two buildings (Lee [5]). These models used the simple k-ϵ turbulence model in the Reynolds-averaged Navier-Stokes (RANS) equations to determine the mean flow and turbulence and, hence, were basically nonlinear flow models solved using either finite difference, finite element, or finite volume solution techniques. Computational fluid dynamics (CFD) models have also been applied to describe the flow within a specific urban structure (e.g., urban street canyon). In particular, Hunter et al. [6] have used the k-ϵ model of turbulence to describe the three-dimensional characteristics of flow regimes within an urban canyon.

Generally speaking, urban flow and dispersion within various arrays of obstacles are addressed on a case-by-case basis. From a theoretical point of view, the problem appears to be complex and unwieldy and there appears to be no idealized starting point for analysis. From an applications point of view, it is easy to get lost in the complexities of particular cases without ever having to see that there are common structures underlying the entire subject. However, from a numerical viewpoint, it appears that the numerical simulation models based on RANS equations are general enough to be applied *mutatis mutandi* to the

problem of disturbed flow within building clusters where mutual flow interferences between buildings need to be taken into account. The principal problem with the application of such CFD models to arrays of buildings is that there is currently very little benchmark mean flow and turbulence data that could be used to compare with the model predictions. In this regard, it should be stressed that CFD modeling applied to a particular problem always yields an answer. For example, we could apply a simplistic turbulence model to a complicated problem and get an answer. It may be a poor answer, but it is an answer nonetheless, and there is no "alarm" automatically warning the user that a particular turbulence closure may be applied outside its realm of applicability. For this reason, it is crucial that before any CFD model with its attendant turbulence closure is applied to a particular class of problems (e.g., flow through an array of buildings), that the model predictions are subjected first to critical and comparative judgements against high-quality data sets before such model predictions are taken as "ground truth".

In this report, we use the standard k-ϵ model of turbulence with a linear eddy viscosity model to simulate the separated flow associated with a two-dimensional array of surface-mounted obstacles set within a turbulent boundary-layer under neutrally-stratified flow. We show a detailed comparison with a wind tunnel experiment of the average flow fields and turbulence kinetic energy for this obstacle array. These results are of more than theoretical interest since they provide information that can be used to interpret the data from this wind tunnel experiment and to ascertain basic phenomenological aspects of the experiment which are not apparent from the laboratory data.

The wind tunnel experiment

The wind tunnel experiment is fully described by Brown et al. [7] and only the important details of the experiment will be presented here. The experiments were conducted in an open-return type wind tunnel at the U. S. Environmental Protection Agency's Fluid Modeling Facility. This wind tunnel has a working test section of length 18.3 m, width 3.7 m, and an adjustable roof of height approximately 2.1 m to eliminate streamwise pressure gradients and allow for a non-accelerating free stream flow.

A schematic of the two-dimensional building array used for these wind tunnel experiments is shown in Figure 1. This array consisted of seven rectangular blocks, each block with equal height, H, and length, L, of 150 mm. The blocks were spaced H apart in the streamwise direction. The streamwise, cross-stream, and vertical velocity components were measured with a pulsed wire anemometer using a pulsing rate of 10 Hz and a sampling time of 120 s at each measurement location. The pulsed wire anemometer, unlike a standard X-array hot-wire anemometer, can be used to measure velocities in high intensity turbulence with reversing flows such as that which exists within an array of obstacles.

Measurements of the three components of the instantaneous velocity were made at 1016 coordinate positions. These measurements consisted of 81 vertical profiles of mean velocity, turbulence velocity variance, and turbulence kinetic energy. These profiles extended from $3.5H$ upstream of the first building to $7.5H$ downstream of the last building. Each vertical profile consisted of either 8 (over the rooftops) or 16 (over the urban canyons, and either upstream or downstream of the array) measurement positions up to a vertical height of $3H$ above the ground surface. All streamwise distances are measured relative to the location of the upstream wall of the first building at $x/H = 0$.

This page intentionally left blank

Numerical simulation

Governing equations, turbulence closure, and boundary conditions

For flow near and through an array of obstacles, we solve the Reynolds-averaged equations for continuity and momentum for steady, incompressible flow. These equations are as follows:

$$\frac{\partial U_i}{\partial x_i} = 0, \tag{1}$$

and

$$\frac{\partial (U_i U_j)}{\partial x_j} = -\frac{\partial P}{\partial x_i} + \frac{\partial}{\partial x_j}\left(\nu \frac{\partial U_i}{\partial x_j} - \langle u_i' u_j' \rangle\right). \tag{2}$$

Here, U_i and u_i' are the mean and fluctuating velocities in the x_i-direction, respectively, P is the kinematic pressure, ν is the kinematic fluid viscosity, and $\langle \cdot \rangle$ denotes the ensemble-averaging operation. In Equations (1) and (2), the convenient Einstein summation convention is assumed, which prescribes that if any of the indices is repeated in a term, a summation over that index is implied. Subscripts 1, 2, and 3 refer to directions along x (streamwise) , y (spanwise), and z (vertical), respectively; averaged quantities are in capital letters or are designated by angle brackets. The presence of the Reynolds stresses, $\langle u_i' u_j' \rangle$, in the mean momentum equations [Equation (2)] implies that the latter are not closed, viz. they contain more unknown quantities than there are equations. Closure requires that some approximations be made in prescribing the Reynolds stresses in terms of the mean flow quantities. The most popular statistical turbulence closures are linear eddy viscosity/gradient transport models that assume a linear relationship between turbulent stresses and mean velocity gradients:

$$-\langle u_i' u_j' \rangle = \nu_t \left(\frac{\partial U_i}{\partial x_j} + \frac{\partial U_j}{\partial x_i}\right) - \frac{2}{3} k \delta_{ij}, \tag{3}$$

where ν_t is the kinematic eddy (turbulent) viscosity and $k \equiv \frac{1}{2}\langle u_i' u_i' \rangle$ is the turbulence kinetic energy (TKE). Substituting Equation (3) into Equation (2) leads to the following closed form for the momentum equation:

$$\frac{\partial (U_i U_j)}{\partial x_j} = -\frac{\partial \Pi}{\partial x_i} + \frac{\partial}{\partial x_j}\left((\nu + \nu_t)\frac{\partial U_i}{\partial x_j}\right), \tag{4a}$$

where

$$\Pi \equiv P + \frac{2}{3} k \tag{4b}$$

is the augmented pressure.

The kinematic eddy viscosity, ν_t, is on dimensional grounds the product of a turbulence length scale, λ, and a turbulence velocity scale, u_0. In the standard k-ϵ turbulence model, the turbulence velocity and length scales are determined as $u_0 = C_\mu^{1/4} k^{1/2}$ and $\lambda = u_0^3/\epsilon$ where ϵ is the dissipation of turbulence kinetic energy and C_μ is a closure constant. Combining the turbulence length and velocity scales, we obtain the familiar expression for the eddy viscosity

$$\nu_t = C_\mu \frac{k^2}{\epsilon}. \tag{5}$$

The standard model uses the following transport equations for k and ϵ:

$$\frac{\partial (U_j k)}{\partial x_j} = \frac{\partial}{\partial x_j}\left[\left(\nu + \frac{\nu_t}{\sigma_k}\right)\frac{\partial k}{\partial x_j}\right] + \nu_t\left(\frac{\partial U_i}{\partial x_j} + \frac{\partial U_j}{\partial x_i}\right)\frac{\partial U_i}{\partial x_j} - \epsilon, \tag{6a}$$

and

$$\frac{\partial (U_j \epsilon)}{\partial x_j} = \frac{\partial}{\partial x_j}\left[\left(\nu + \frac{\nu_t}{\sigma_\epsilon}\right)\frac{\partial \epsilon}{\partial x_j}\right] + C_{1\epsilon}\frac{\epsilon}{k}\nu_t\left(\frac{\partial U_i}{\partial x_j} + \frac{\partial U_j}{\partial x_i}\right)\frac{\partial U_i}{\partial x_j} - C_{2\epsilon}\frac{\epsilon^2}{k}. \tag{6b}$$

The equations contain five closure constants; namely, C_μ, σ_k, σ_ϵ, $C_{1\epsilon}$, and $C_{2\epsilon}$. The standard k-ϵ model employs values for constants that are arrived at by comprehensive data fitting over a wide range of turbulent flows [8]:

$$C_\mu = 0.09; \quad \sigma_k = 1.00; \quad \sigma_\epsilon = 1.30; \quad C_{1\epsilon} = 1.44; \quad C_{2\epsilon} = 1.92. \tag{7}$$

The turbulent diffusion of k and ϵ in Equations (6a) and (6b), respectively, are represented using a gradient diffusion hypothesis with the Prandtl numbers σ_k and σ_ϵ used to connect the eddy diffusivities of k and ϵ to the eddy viscosity ν_t.

Since the computational domain is chosen to be large compared with the two-dimensional array of obstacles, the flow at its boundary is not affected by any of the obstacles. Hence, free boundary conditions are imposed at all air-to-air boundaries in the flow domain. At the inflow boundary, the measured distributions of streamwise mean velocity, $U \equiv U_1$, the vertical mean velocity, $W \equiv U_3 = 0$, and the turbulence kinetic energy, k, are used. This information is obtained from the vertical profiles of U and k measured furthest upstream from the upstream face of the first building (viz., at $x/H = -3.5$, or $x = -500$ mm, where $x = 0$ corresponds to the upstream wall of the first building). Above $z = 3H$, measurements for U and k are not available; and, for the inflow boundary conditions, the vertical profile of U above $z = 3H$ was assumed to adhere to a power-law profile with an exponent of 0.16 (corresponding to a nominal neutral boundary layer simulated in the wind tunnel using spires [7]), and the vertical profile of k was assumed to be constant above $z = 3H$

(corresponding, as such, to a deep constant stress layer). Unfortunately, at the inflow, ϵ was not measured and, consequently, estimated simply as $\epsilon = k^{3/2}/l$ where the dissipation length scale l was chosen as approximately $1.2H$. The length scale l is unknown at the inflow boundary, but variation of its value from $0.1H$ to $1.2H$ showed that it had only a very small impact on the final solution. Far downstream, at the outflow boundary, we set $\partial U/\partial x = \partial k/\partial x = \partial \epsilon/\partial x = W = 0$. At the upper boundary, we set $\partial U/\partial x = W = 0$, $\partial k/\partial z = \partial \epsilon/\partial z = 0$.

At all solid boundaries (ground, obstacle walls, obstacle roofs) in the computational domain, wall functions are used for mean velocities and turbulence quantities. The implementation of the wall boundary conditions starts with the evaluation of

$$n_P^+ = \frac{n_P}{\nu}\left(\frac{\tau_w}{\rho}\right)^{1/2}, \tag{8}$$

where n_P is the normal distance of the near wall node P to the solid surface (ground, wall, or roof), τ_w is the shear stress at the wall, and ρ is the fluid density. It is assumed that the first grid point closest to the solid surface is located in the logarithmic region, $30 < n_P^+$, where the flow is in local equilibrium (viz., the production is exactly balanced by the dissipation). In this case, $u_* \equiv \sqrt{\tau_w/\rho}$ is given by

$$u_* = C_\mu^{1/4} k_P^{1/2}, \tag{9a}$$

and

$$u_P^+ \equiv \frac{v_{t,P}}{u_*} = \frac{1}{\kappa}\ln(E n_P^+), \tag{9b}$$

where κ is von Karman's constant ($\kappa \approx 0.41$ for smooth and rough surfaces), $v_{t,P}$ is the mean velocity parallel to the wall at the near wall node P, $n_P^+ \equiv u_* n_P/\nu$ is the dimensionless distance from the wall at the near wall node P, and E is the wall roughness parameter which for a hydrodynamically smooth wall assumes the value $E = 9.793$ [9] (obtained from correlation of measurements for smooth surfaces). In the current simulations, all the solid surfaces are assumed to be smooth. The wall boundary condition for the tangential velocity requires a relationship between the velocity at the first grid point above the wall and the wall shear stress, which in accordance to Equations (9a) and (9b), can be expressed as

$$\tau_w = \rho u_*^2 = \rho C_\mu^{1/4} k_P^{1/2} \frac{\kappa v_{t,P}}{\ln(n_P^+ E)}. \tag{10}$$

Finally, the TKE dissipation rate at the first grid point P above the wall can be set to the value

$$\epsilon_P = \frac{u_*^3}{\kappa n_P} = \frac{C_\mu^{3/4} k_P^{3/2}}{\kappa n_P}. \tag{11}$$

Numerical method

Our computational domain for simulating the two-dimensional array of buildings used in the wind tunnel experiment (cf. Figure 1) extended in the streamwise direction from $x/H = -5$ to $x/H = 15$, with the upstream wall of the first building at $x = 0$. The height of the domain was $9H$. The results of the numerical simulation reported below were obtained with an orthogonal 251×51 grid shown in Figure 2. The grid lines were concentrated near the solid surfaces (ground, rooftop, and building walls) and the spacing between grid lines was gently stretched at increasing distances from the solid surfaces.

The numerical method employs a structured, non-orthogonal (allowing boundary-fitted coordinates), fully colocated (viz., all flow variables are stored at the same location), cell-centered, finite volume approach for the discretization of the computational domain. Within this non-orthogonal system, the velocity vector is decomposed into its Cartesian components, and these are the components to which the momentum equations relate. Advective volume face fluxes are approximated using the upwind discretization scheme, and physical diffusive cell fluxes are approximated using a conventional second-order central differencing scheme. The SIMPLE algorithm [10] was used for pressure correction. Here, mass continuity is enforced by solving a pressure correction equation which, as part of the iterative sequence, steers the pressure toward a state at which all mass residuals in the cells are negligibly small. In conjunction with the colocated grid use here, this method is known to provoke chequerboard oscillations in the pressure field, reflecting a state of pressure-velocity decoupling. To avoid this, the widely used method of Rhie and Chow [11] is adopted to non-linearly interpolate the cell face velocities from the nodal values (at the center of the cells). The interpolation scheme essentially introduces a fourth-order pressure diffusion correction that smooths out the pressure if it oscillates rapidly. In the numerical scheme, the transport equations for the mean velocity, turbulence kinetic energy, and viscous dissipation rate and the pressure-correction equation are solved sequentially and iterated to convergence, defined by reference to the sum of the absolute cell residuals for mass and momentum components. Stone's strongly implicit procedure [12] was applied to solve the system of algebraic equations arising from the discretization of the transport equations and pressure-correction equation. Iterative refinement of all fields was continued until the sum of the absolute cell residuals for mass and for momentum was satisfied to within 0.1% of the total mass and momentum fluxes, respectively, at the inflow boundary. For the current simulation, this required about 780 outer iterations which took approximately 210 s on an 800 MHz Pentium III PC.

Results and discussion

Mean streamwise velocity

Figure 3 compares model predicted vertical profiles of the mean streamwise velocity U at six fixed x-locations covering the range $-2.5 \leq x/H \leq -0.1$ in the impingement zone directly upstream of the first building. At $x = -225$ mm and -150 mm, the wind speed reduction below about $z = 2H$ relative to the far upstream profile is well predicted by the model, although the wind speeds below about $z/H = 1/3$ are slightly over-estimated. At $x = -75$ mm and -38 mm, the wind speed reduction below and wind speed increase above the level $z/H \approx 4/3$ relative to the upstream profile is reproduced well. However, the reverse flow near the surface at these x-positions is underestimated by the model. In particular, streamfunction contours of the recirculation zone (not shown) in front of the first building indicate that the predicted reattachment length of this zone occurs at $z/H \approx -0.33$, whereas the measurements suggest that the reattachment occurs at about $z/H \approx -0.52$. Close to the upstream wall of the first building at $x = -15$ mm, the significant wind speed reduction below the building height H owing to the adverse pressure rise (horizontal pressure gradient) upstream of the solid obstacle is modeled well, as is the moderate speed-up above the building top.

Figure 4 shows vertical profiles of the mean streamwise velocity U at five fixed x-locations ($0.1 \leq x/H \leq 0.9$) over the roof of the first building. Generally speaking, the speed-up over the roof compared with the reference upwind profile and the presence of a thin separation zone near the roof surface with flow reversal is well matched between the predictions and the measurements, although the magnitude of the reversed flow is underestimated slightly. Figure 5 shows reasonable agreement between the measurements and the model predictions of U at various fixed x-locations within the first urban canyon ($1.1 \leq x/H \leq 1.9$). An important feature captured by the model predictions is the very strong shear layer that forms immediately downstream of the rear face of the first building, whose signature is revealed in the inflection point in $U(z)$ at or near the building height H. Note that the high values of mean shear $\partial U/\partial z$ just above building height over the first urban canyon (Figure 5) are reproduced well by the model. The speed-up above about $z/H \approx 4/3$ is predicted correctly over the first urban canyon, although the magnitude of the reverse flow in the canyon below about $z/H \approx 2/3$ is underestimated slightly. The reverse velocity on the underside of the standing vortex within the canyon is comparable to the forward velocity at the canyon top, and this feature appears to be reproduced by the model predictions.

Figure 6 compares computed and measured mean streamwise velocity U at five x-stations over the rooftop of the second building ($2.1 \leq x/H \leq 2.9$). Again, wind reduction below and moderate speed-up above about $z/H \approx 4/3$ is well predicted. The model predicts that no separation occurs over the second rooftop (in contrast to the behavior over the first rooftop) which accords well with the observations. Vertical profiles of U at five x-locations within the second urban canyon ($3.1 \leq x/H \leq 3.9$) and over the rooftop of the third building ($4.1 \leq x/H \leq 4.9$) are displayed in Figures 7 and 8, respectively. Note that the predicted magnitude of the wind shear over the second urban canyon is larger than what is observed in the wind tunnel measurements. The primary reason for this discrepancy appears to be the reduced vertical turbulent diffusion of shear stress in the high shear layer bordering the urban canyon top—a defect manifesting itself by the greater level of shear strain in this area than observed. The reduced vertical turbulent diffusion results from the underestimation of the turbulence kinetic energy, which implies an underestimation in the turbulent viscosity. Because of this, the high shear layer generated near the urban canyon top dissipates more slowly in the streamwise direction along the canyon and the succeeding rooftop than in the wind tunnel (cf. Figures 7 and 8). In consequence, the prediction of speed-up above and wind reduction below the level $z/H \approx 4/3$ is slightly over-predicted and under-predicted, respectively.

Vertical profiles of both the computed and measured mean streamwise velocity U within the third urban canyon and the fourth rooftop are almost identical to the profiles obtained, respectively, for the second urban canyon (Figure 7) and the third rooftop (Figure 8). In consequence, U appears to have reached streamwise equilibrium (i.e., the mean streamwise velocity field is fully developed) by the second canyon, a feature that both the wind tunnel measurements and the numerical simulation agree on. Within the array interior ($x \gtrsim 3H$), it appears that the mean streamwise velocity within the second urban canyon and above third rooftop should be "typical" of their neighbors (viz., there is little variation in the amplitude of the streamwise wind speed modulation from one building to the next), and that in the array interior a periodic boundary-condition might have been used to model the flow in a single representative building and urban canyon.

Figures 9 and 10 compare computed and measured mean streamwise velocity U in the exit region of the array directly downstream of the last building covering the range $13.1 \leq x/H \leq 20.5$. The vertical profile of U at $x = 1965$ mm lies just 15 mm downstream of the rear wall of the last building. Below the building height H, the vertical profile of U at this x-location exhibits essentially no shear (i.e., $\partial U/\partial z \approx 0$) and this absence of shear is reproduced well by the model predictions as is the high value of mean shear at or near the building height H. The model predicts the existence of a recirculation zone behind the last building with a

reattachment point at $x \approx 2475$ mm, which is in good conformance with the observations. Further downstream, in the far wake region, the vertical profiles of U are recovering towards the far upwind reference state. It is seen that the model underpredicts slightly the rate of momemetum recovery in this region. It is interesting to note that even at the furthest downstream measurement location (at $x/H = 20.5$ or at $x/H = 7.5$ downstream of the last building), the streamwise mean velocity has still not recovered to its upwind equilibrium state.

Mean vertical velocity

Comparisons of measured and modeled vertical profiles of the mean vertical velocity W, at six fixed x-positions covering the range $-2.5 \leq x/H \leq -0.1$ in the impingement zone directly upstream of the first building, are shown in Figure 11. As the front face of the first building is approached, the vertical velocity is positive as air is forced up and over the building. This feature in the observations is reproduced well by the modeled results, as is the position and magnitude of the maximum positive vertical velocity at or near the top of the building (viz., at $z/H \approx 1$). For $x \gtrsim -38$ mm, the downward (negative) vertical velocity below about $z/H \approx 2/3$, resulting from the flow hitting the front face of the obstacle and flowing downwards to create the region of reversed flow in front of the first building, is underestimated, especially closer to the front face (e.g., compare measured and computed results for $x = -15$ mm in Figure 11). Indeed, in front of the first building, the model predicts that there is a vertical pressure gradient with a high pressure region centered at about $z/H \approx 2/3$ that forces the air over the first building above this level and down towards the ground below this level. This prediction appears to be in good conformance with the measurements of the mean vertical velocity.

Profiles of measured and computed mean vertical velocity W covering the range $0.1 \leq x/H \leq 0.9$ over the rooftop of the first building are given in Figure 12. The upward motion of air above the first building rooftop agrees well with the wind tunnel measurements. The thin separation zone and negative vertical velocity in this zone is captured in the numerical simulation. It should be noted that the streamline curvature over the first building rooftop as well as immediately upstream of this rooftop is concave upwards, implying a destabilising (exhange-enhancing) influence on the turbulence. This feature of the flow curvature is reproduced in the model predictions. Figure 13 compares computed and observed vertical profiles of W for five fixed x-stations ($1.1 \leq x/H \leq 1.9$) within the first street canyon. The prediction that the downward (negative) vertical velocity on the downstream end of

the street canyon is larger in magnitude than the upward (positive) vertical velocity on the upstream end of the canyon is in conformance with the observations. However, the magnitude of both the upward and downward vertical velocities are under-predicted by the model, with the degree of under-prediction being larger closer to the canyon walls.

Measured and modeled vertical profiles of W over the second building rooftop are exhibited in Figure 14 for x-stations in the range $2.1 \leq x/H \leq 2.9$. In contrast to the positive vertical velocity over the first building rooftop, there is a weak downward vertical motion over the second rooftop arising from the slight downward curvature (implying a stabilizing or exchange-suppressing influence) of the mean flow streamlines above the upstream edge of the second building. This feature in the flow is well reproduced in the numerical simulations. Figures 15 and 16 display, respectively, vertical profiles of W over the second street canyon ($3.1 \leq x/H \leq 3.9$) and the third building rooftop ($4.1 \leq x/H \leq 4.9$) in comparison with the simulation using the present model. With reference to Figures 13 and 15, it is seen that strength of the vortex in the second urban canyon is smaller than that in the first canyon in the sense that vertical motions are stronger in the first canyon than in the second canyon. This feature is captured in the numerical simulation, although the magnitude of the upward motion on the upstream side and downward motion on the downstream side is under-predicted in the second canyon. However, the degree of under-prediction is not as severe as it was for the first street canyon (cf. Figure 13). Nevertheless, the locations of the peak upward and downward vertical velocities in the street canyons appear to be well predicted. The mean flow streamlines over the third building rooftop are essentially horizontal and there is negligible vertical mean velocity over this rooftop. This aspect of the flow is represented well in the numerical simulations (cf. Figure 16).

Vertical profiles of both the computed and measured mean vertical velocity W within the third street canyon and over the fourth building rooftop are identical (approximately or better) to the profiles obtained, respectively, within the second street canyon (Figure 15) and the third rooftop (Figure 16). Hence, in conformance with the behavior of U, the mean vertical velocity field appears to be fully established by the second urban canyon within the array interior, a feature of the flow that is in good overall conformance with the model predictions.

Figures 17 and 18 compare computed and measured profiles of mean vertical velocity W in the exit region of the array directly downstream of the last building covering the range $13.1 \leq x/H \leq 20.5$. Generally speaking, computed and measured W over the range of the exit region for which observations are available differ by less than about 5%, except within the recirculation bubble at $x = 1965$ and 1988 mm. In particular, the upward vertical

motion just downstream of the last building in the recirculation zone is overestimated by about 80%. The prediction of the weak downward vertical motion just upstream of the reattachment point is in good conformance with the measurements. Finally, the rate of recovery of the vertical mean momentum beyond the reattachment point in the far wake region to its far upstream reference state is reproduced accurately.

Turbulence kinetic energy

Figure 19 presents vertical profiles of turbulence kinetic energy, k, in the impact region upstream of the first building at the same x-stations as the mean velocity field described above ($-2.5 \leq x/H \leq -0.1$). Although the increase in k above the building height H as the building is approached is reasonably well predicted, the positions of the maximum k for $x \gtrsim -75$ mm (i.e., in the region of recirculation zone just ahead of the front face of the first building) are too far away from the ground surface. This feature seems to be accompanied by a second defect in the model predictions (perhaps indirectly provoked by the first in the upward shift of the position of maximum turbulence generation)—namely, an insufficient level of turbulence energy near the ground surface ($z/H \lesssim 2/3$). A possible explanation for this underestimation in the TKE level within the impingement zone is that the linear eddy-viscosity model used with the k-ϵ turbulence model cannot capture the particularly high-level of normal-stress anisotropy expected to occur in this region. This failure to properly capture the normal-stress anisotropy in the impingement zone will have two effects on the production of TKE. Firstly, the normal stress anisotropy is responsible for the production of shear stress $-\langle u'w' \rangle$ which in the streamline coordinate system (i.e., the streamlines and their orthogonal trajectories define the orthogonal coordinate net) takes the form $(2\langle u'^2 \rangle - \langle w'^2 \rangle)U/R$ (R is the local radius of streamline curvature), which in the impingement zone would correspond to a gain in $-\langle u'w' \rangle$ owing to the positive (unstable) flow curvature ($R > 0$) in this region (noting that $2\langle u'^2 \rangle \gg \langle w'^2 \rangle$). Hence, a reduction in normal-stress anisotropy would lead to an underestimation in $-\langle u'w' \rangle$, which in turn would lead to a reduced shear stress production, $-\langle u'w' \rangle \partial U/\partial z$, of the TKE. Secondly, an underestimation of the normal-stress anisotropy will lead to an under-prediction of the normal stress production of k, $-(\langle u'^2 \rangle - \langle w'^2 \rangle)\partial U/\partial x$, in the impingement zone in front of the first building. Note that in this region $\partial U/\partial x < 0$ owing to the deceleration of the flow in front of the windward face of the first building (induced by the adverse horizontal pressure gradient here), so the term (in streamline coordinate system) $-(\langle u'^2 \rangle - \langle w'^2 \rangle)\partial U/\partial x$, corresponds to a gain in TKE.

Figure 20 presents a comparison of measured and modeled profiles of k for five x-locations

($0.1 \leq x/H \leq 0.9$) over the first building rooftop. The model predicts a monotonic increase of the turbulence level (and, hence, a steady production of turbulence energy) in the streamwise direction along and near the rooftop surface. This feature largely conforms with the wind tunnel simulations. However, the maximum TKE level is underestimated in the numerical simulations. The impingement process occuring in front of the first building wall also provokes severe concave (unstable) flow curvature in the region of the flow immediately upstream of the first building rooftop. It is expected that the turbulence kinetic energy in this region will increase significantly due to the cumulative effect of concave streamline curvature as fluid elements are forced up and over the first building. Indeed, the curvature term (in streamline coordinates) $-\langle u'w' \rangle U/R$ is a source of production of k in this region of positive (unstable) R. Furthermore, the region of concave streamline curvature extends over the first building rooftop. The subtle effect of curvature strain on turbulence does not appear to be captured in the present model and, hence, may explain differences in the TKE levels over the first building rooftop between the model predictions and measurements. Alternatively, the observed large peak in the TKE just above the first building rooftop can be also interpreted as arising from an oscillation of the high shear layer by the larger-scale upstream turbulence which would enhance $\langle u'^2 \rangle$ (and, hence k) as the probe at this level records high and low velocities as the shear zone flaps upwards and downwards. The fact that such a large peak is missing in the predictions may suggest that this process is not well represented in the k-ϵ turbulence model. Since TKE is exported downstream by local advection and turbulent transport, an underestimation of the TKE level in the region just upstream of the first building will lead generally to an underestimation of the TKE level all positions downstream of the location of strong turbulence generation.

Figure 21 compares computed and measured vertical profiles of k within the first street canyon for x-stations in the range $1.1 \leq x/H \leq 1.9$. The position of the prominent "nose" in the k profiles lying just above the street canyon top is largely reproduced by the numerical simulation, albeit the peak value of k is significantly underestimated. This defect is a consequence of the under-prediction of the TKE level upstream of this region owing to the inability of the present model to account properly either for the effects of secondary strain on the turbulence and/or for the effects of the large-scale flapping of the strong shear layer at the canopy top. Just downstream of the first building rooftop and on the upstream side of the first street canyon (e.g., at $x = 165$ mm), there is a thin intense shear layer where the turbulence energy is large. Moving downstream of this position, the evolution of the TKE profiles is dominated by the vertical spreading of this shear or mixing layer. At the center of this layer lying just above the building height H, the peak value of TKE attenuates downstream, whereas regions above and below the peak "import" turbulence energy by outward pressure or turbulent transport from the core of the shear layer, causing

an increase in the turbulence energy in these regions. These characteristics of the flow are largely reproduced by the numerical simulation. Furthermore, the downstream advection and vertical diffusion of TKE results in a larger level of turbulence energy being found on the downstream side of a street canyon than the upstream side, a feature that is also present in the model predictions. Within the street canyon, minimum levels of TKE are found on the upstream side of the canyon (protected region) where the TKE is essentially independent of height. These features are reproduced in the simulations, although the near constant TKE level on the upstream side of the canyon is underestimated by the model. Finally, it appears that the rate of vertical spreading of the shear or mixing layer in the numerical simulation is smaller than in the measurements. This discrepancy may be the result of an underestimation of the turbulent viscosity ν_t [cf. Equation (5)] owing to the smaller predicted TKE levels.

Figures 22 and 23 exhibit the comparison of the predicted values of TKE with experimental data, respectively, over the second building rooftop and the second street canyon for the same x-stations as the mean velocity field described above. In contrast to the behavior over the first building rooftop, the peak turbulence energy decreases monotonically (approximately or better) as one moves downstream across the second building rooftop. Such a feature was not found in the numerical simulations. This observed property of the flow may be the result of streamline curvature on TKE production. Specifically, the reduced production (loss) of TKE along the second building rooftop arises from two effects: (1) the TKE production term due to curvature strain, $-\langle u'w'\rangle U/R$, represents a (negative) loss term in this region of negative (stable) R (viz., the downward or convex curvature of the mean streamlines over the second rooftop suppresses the turbulence here); and, (2) the reduction of the shear stress $-\langle u'w'\rangle$ due to convex streamline curvature will lead to reduced shear production. Again, it is seen that the subtle effect of curvature strain on the turbulence is not adequately captured by the present model. All the qualitative features of the turbulence energy profiles are predicted moderately well in the third street canyon, although the TKE levels are underestimated at all vertical levels. However, the degree of underestimation is not as great as it was for the first street canyon.

Comparisons of computed and measured profiles of k over the third, fourth, fifth, and sixth building rooftops and street canyons are presented in Figures 24 to 31. Figure 32 compares computed TKE profiles with measured ones over the seventh building rooftop. Unlike the mean velocity field which achieves streamwise equilibrium in the array interior when the flow reaches the third building, the TKE never seems to reach streamwise equilibrium and, consequently, exhibits downstream development throughout the entire array interior. Interestingly, the level of TKE over the rooftops in the array interior change negligibly as

one moves in the streamwise direction across the rooftops, suggesting that there is a local equilibrium established here between the production and dissipation of TKE. In contrast, the peak TKE levels decrease monotonically as one moves downstream from the upstream to the downstream side of the street canyons as the TKE in the shear layer above the building top is "exported" by turbulent diffusion into the canyons. Furthermore, the TKE levels in street canyons further downstream are successively smaller owing to the fact that the peak TKE in the mixing layer above each canyon attenuates downstream (and, hence, there is less TKE available to transport into each successive street canyon downstream). These qualitative features of the flow are largely reproduced by the numerical simulation. The quantitative agreement between the computed and measured TKE profiles generally improve with increasing downstream distance.

Figures 33 and 34 compare computed and measured TKE profiles in the exit region of the array directly downstream of the last building covering the range $13.1 \leq x/H \leq 20.5$. Overall, the TKE profiles in the exit region appear to be very similar in shape, and all the qualitative features in these profiles appear to be correctly predicted; the quantitative agreement is also fairly good. Just downstream of the last obstacle and below the building height at $x = 1965$ and 1988 mm (cf. Figure 33), the turbulence energy is practically eliminated within this sheltered "quiet" zone, a feature that is correctly reproduced by the model. For the profiles in the range from 2025 to 2775 mm, the position of the maximum TKE is correctly predicted. This position corresponds to the center of the curved shear layer that bounds or envelops the recirculation zone behind the last building. The characteristics of the vertically spreading mixing zone (or, wake zone) above and downstream of the recirculation zone are predicted well by the model. Finally, the rate of recovery of the TKE in the far wake region to the upstream reference condition is reproduced correctly. Even at $x = 3075$ mm or, equivalently, $x/H = 7.5$ downstream of the last building (measurement furthest downstream), the TKE profile has the appearance of a detached mixing layer despite the fact that the mean flow has re-attached at about $x/H = 3.5$ downstream of the last building. This profile form is a residue of the strong shear or mixing layer that detaches from the last building rooftop and spreads outward by pressure or turbulent diffusion until this vertically spreading mixing layer makes contact with the ground surface. This is an example of disequilibrium that results in the TKE profile at even the furthest downstream measurement position not having recovered to the reference far upstream state.

Summary and conclusions

A linear eddy-viscosity k-ϵ turbulence-closure model, applied with wall functions, has been used to calculate the disturbed mean flow and turbulence near and about an array of two-dimensional buildings. The primary purpose of this exercise was to assess critically the model's predictive performance by comparison of the mean flow and turbulence statistics with a very comprehensive and detailed wind tunnel simulation. It should be emphasized that for this numerical simulation, the closure constants in the k-ϵ turbulence model retained their original (standard) values. In consequence, all model predictions were obtained without adjustment any of the closure constants. This ensures that the process did not simply degenerate into a "curve-fitting" exercise .

The comparison of predicted and measured streamwise and vertical velocity profiles indicated that most of the qualitative features of the mean flow field—such as speed-up over the first building rooftop, the presence of a thin separation layer near the surface of the first rooftop and the absence of such a feature in all the succeeding rooftops, the standing vortex in the street canyon, the upward vertical motion on the first rooftop, the downward vertical motion on the second rooftop, the thin strong shear layer that forms at building height, the recirculation zone behind the last building, and the development of the mixing layer above and downstream of this recirculation zone, and the rate of momentum recovery in the far wake region—are correctly predicted. The quantitative agreement is also fairly good throughout most of the flow domain, with the greatest discrepancy in the mean velocity field arising from the prediction of a smaller than observed separation zone in the impingement region upstream of the first building and an underestimation of the magnitude of both the downward vertical velocity on the downstream side and the upward vertical velocity on the upstream side of a street canyon.

The turbulence kinetic energy from the numerical and physical simulations show striking resemblances and, indeed, most of the qualitative features of the turbulence energy as its develops near and through the array of buildings is adequately predicted. In terms of quantitative agreement, it is found that the TKE level is generally underestimated by the model. This underestimation may be caused by the inability of the model to capture the disproportionate and inhomogeneous sensitivity of the Reynolds stress components to secondary strains in the flow, particularly those associated with curvature. Specifically, the production of TKE just upstream and above the first building and across the first building rooftop arising from the mean streamline concave (destabilising) curvature strain acting through the shear stress is not adequately captured by the model. Because the

TKE is exported downstream and vertically by advection and by turbulent and/or pressure diffusion, the under-prediction of the TKE at and near the leading edge of the first building (i.e., the location where the turbulence energy production is greatest) will result in reduced TKE levels at all positions downstream of this location.

The k-ϵ turbulence-closure model with an isotropic, linear eddy viscosity is the simplest complete turbulence model (viz., no advance knowledge of any property of the turbulence is required for the simulation other than the initial and/or boundary conditions for the problem) that is available currently, and its moderately good predictive performance of the complicated developing flow through an array of two-dimensional buildings without the need to adjust any closure constants is encouraging. This model may be useful as a general-purpose simulator of urban flows since it is simple enough to be tractable numerically and, hence, not require excessive computing time. Notwithstanding certain weaknesses of the k-ϵ turbulence model for urban flows as discussed in this report, the model remains attractive because of its formalistic simplicity, numerical robustness, and computational economy. However, before this model (or, variants of it) can be used for this purpose, it needs to be validated against more experimental data for flow in various obstacle arrays. From this perspective, the availability of extensive and accurate experimental data for flow through various obstacle arrays is urgently required.

References

1. Paterson, D. A. and Apelt, C. J. (1986). Computation of Wind Flows Over Three-Dimensional Buildings. *Journal of Wind Engineering and Industrial Aerodynamics*, 24, 193–213.

2. Zhang, Y. Q., Huber, A. H., Arya, S. P. S., and Synder, W. H. (1993). Numerical Simulation to Determine the Effects of Incident Wind Shear and Turbulence on the Flow Around a Building. *Journal of Wind Engineering and Industrial Aerodynamics*, 46 & 47, 129–134.

3. Zhou, Y. and Stathopoulos, T. (1997). A New Technique for the Numerical Simulation of Wind Flow Around Buildings. *Journal of Wind Engineering and Industrial Aerodynamics*, 72, 137–147.

4. Cowan, I. R., Castro, I. P., and Robins, A. G. (1997). Numerical Considerations for Simulations of Flow and Dispersion Around Buildings. *Journal of Wind Engineering and Industrial Aerodynamics*, 67 & 68, 535–545.

5. Lee, R. (1992). A Finite Element/Finite Difference Approach for Modeling Three-Dimensional Flow and Pollutant Dispersion Around Structures. UCRL–J–10775 DE92 019377.

6. Hunter, L. J., Watson, I. D., and Johnson, G. T. (1990/91). Modeling Air Flow Regimes in Urban Canyons. *Energy and Buildings*, 15–16, 315–324.

7. Brown, M. J., Lawson, R. E., Decroix, D. S., and Lee, R. L. (2000) Mean Flow and Turbulence Measurements Around a 2-D Array of Buildings in a Wind Tunnel. *11-th Joint AMS/AWMA Conference on the Applications of Air Pollution Meteorology*, Long Beach, California.

8. Launder, B. E. and Spalding, D. B. (1974). The Numerical Computation of Turbulent Flows. *Comp. Meth. Appl. Mech. Engineer.*, 3, 269–289.

9. Schlichting, H. (1979). *Boundary-Layer Theory*, Seventh Edition, McGraw-Hill, New York.

10. Patankar, S. V. (1980) *Numerical Heat Transfer and Fluid Flow*, Hemisphere Publishing Corporation, New York.

11. Rhie, C. M. and Chow, W. L. (1983). Numerical Solution of the Turbulent Flow Past an Airfoil with Trailing Edge Separation. *AIAA J.*, 21, 1525–1532.

12. Stone, H. L. (1968). Iterative Solution of Implicit Approximations of Multidimensional Partial Differential Equations. *SIAM J. Numer. Anal.*, 5, 530–558.

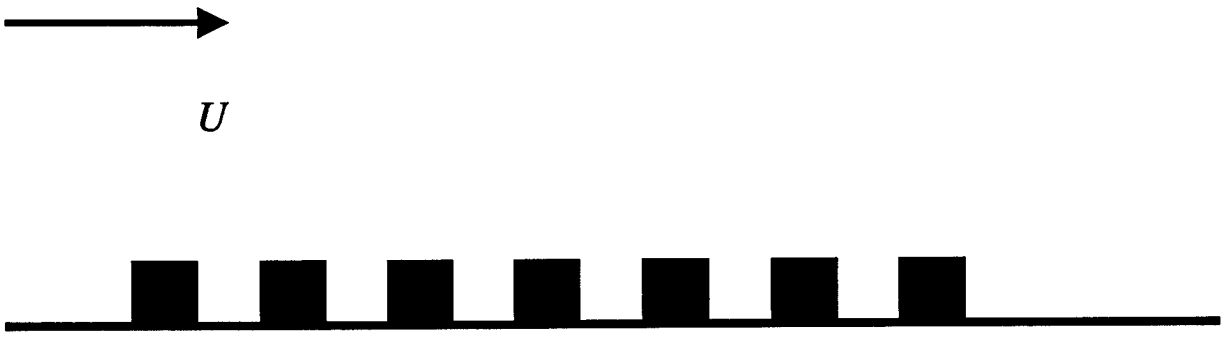

Figure 1. *The two-dimensional building array used in the wind tunnel experiment. The array consisted of rectangular blocks with an equal height and length of 150 mm, with each block extending wall-to-wall across the wind tunnel in the spanwise direction.*

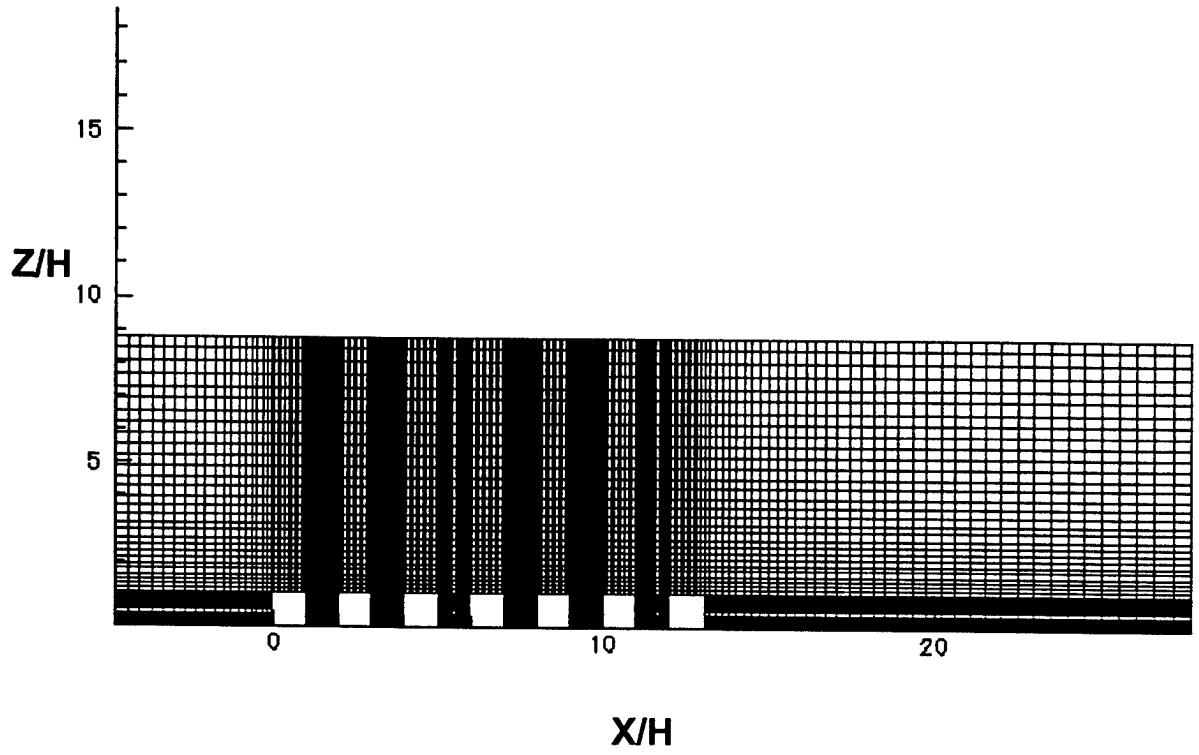

Figure 2. *Computational grid used for numerical simulation of the two-dimensional building array.*

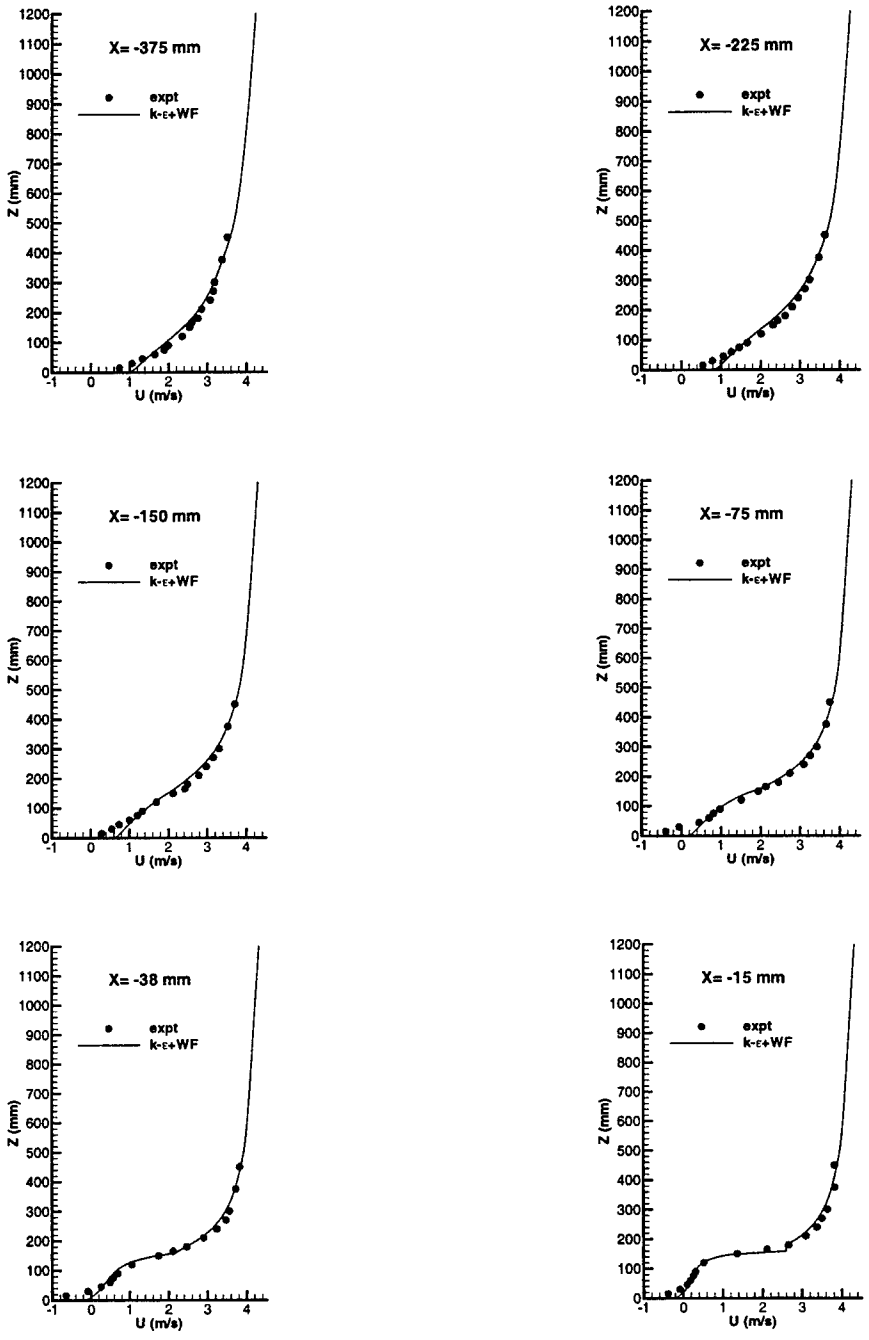

Figure 3. *Vertical profiles of the mean streamwise velocity U at specified x-locations in the impingement zone* (-2.5 <= *x/H* <= -0.1) *upstream of the front face of the first building compared with time-averaged wind tunnel measurements.*

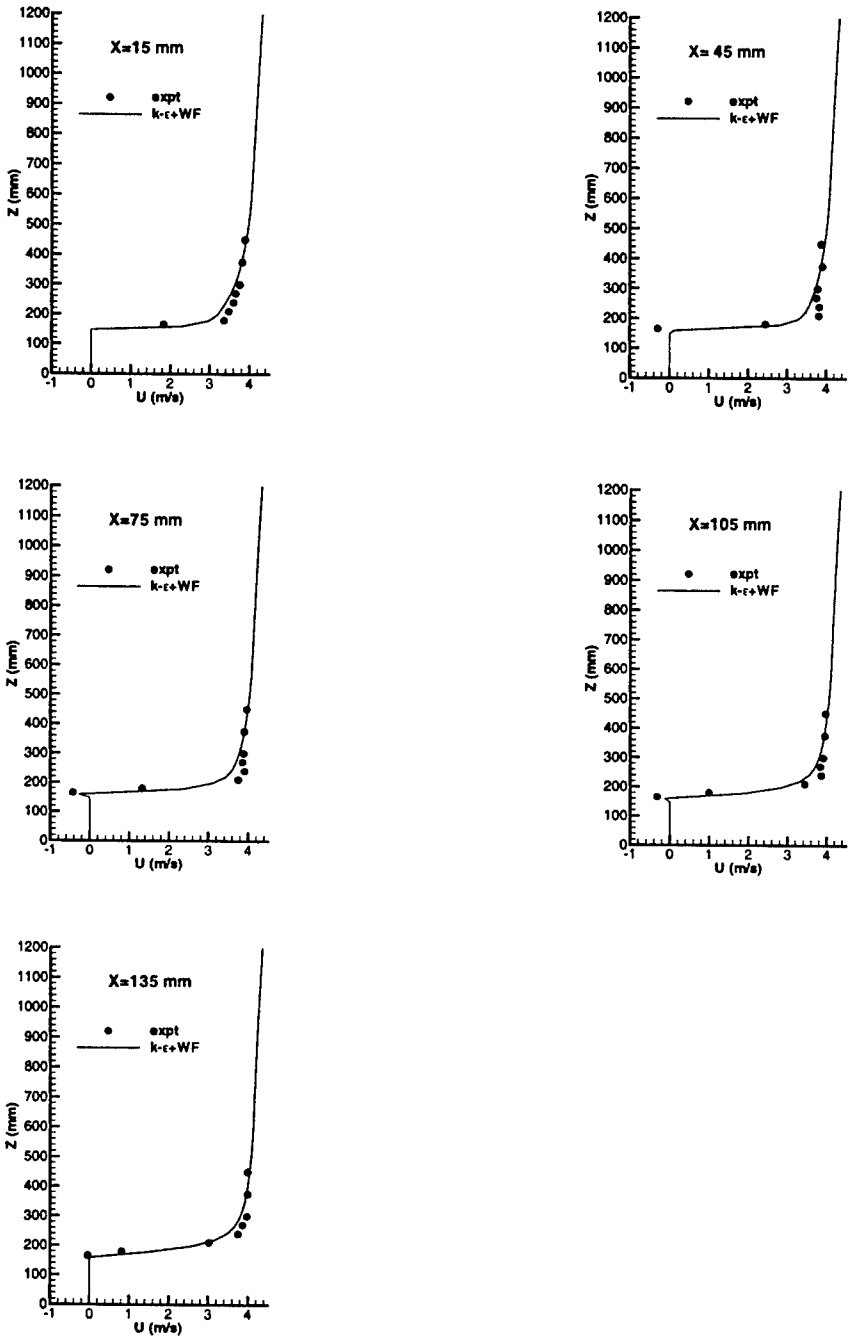

Figure 4. *Vertical profiles of the mean streamwise velocity U at specified x-locations over the roof* (0.1 <= *x/H* <= 0.9) *of the first building compared with time-averaged wind tunnel measurements.*

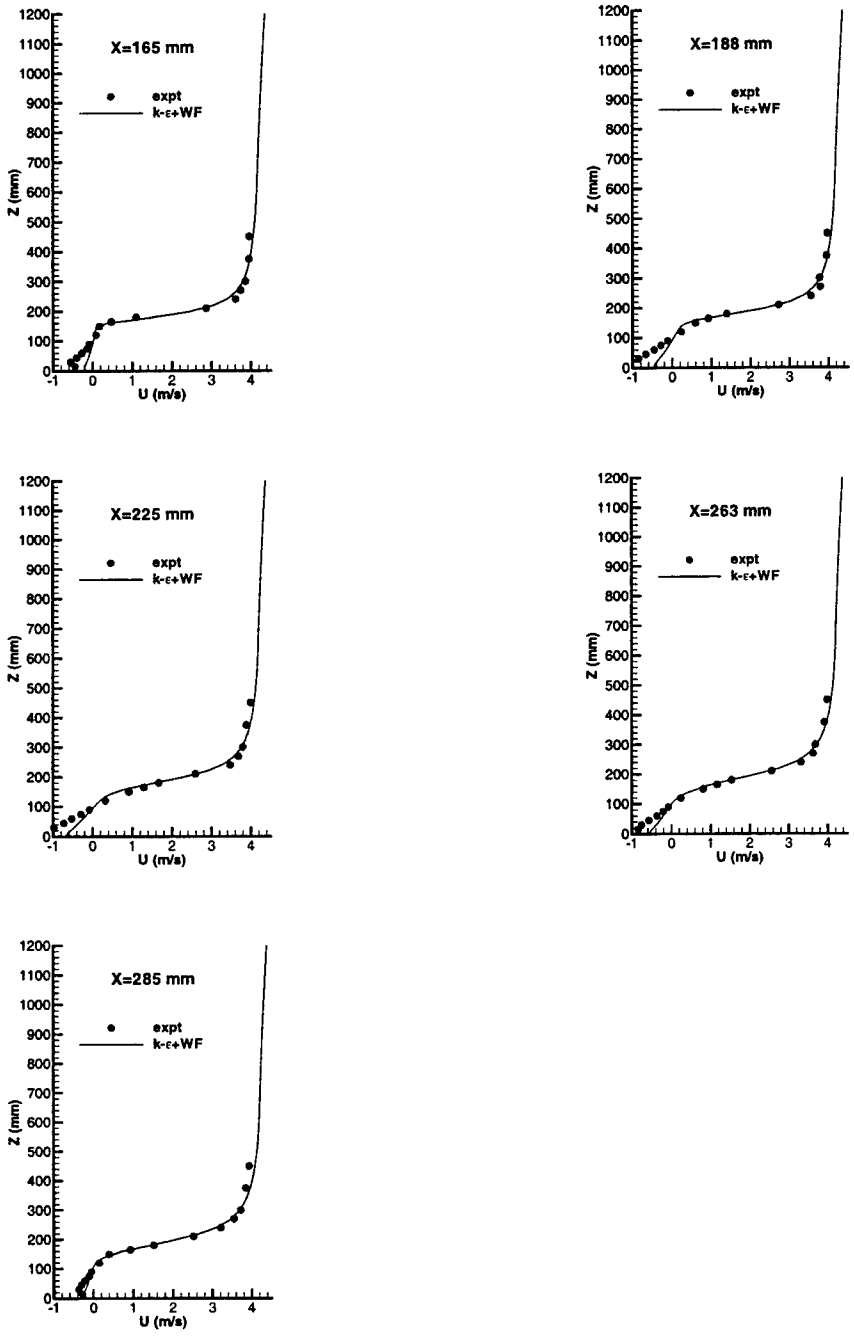

Figure 5. *Vertical profiles of the mean streamwise velocity U at specified x-locations within the first urban canyon* (1.1 <= *x/H* <= 1.9) *compared with time-averaged wind tunnel measurements.*

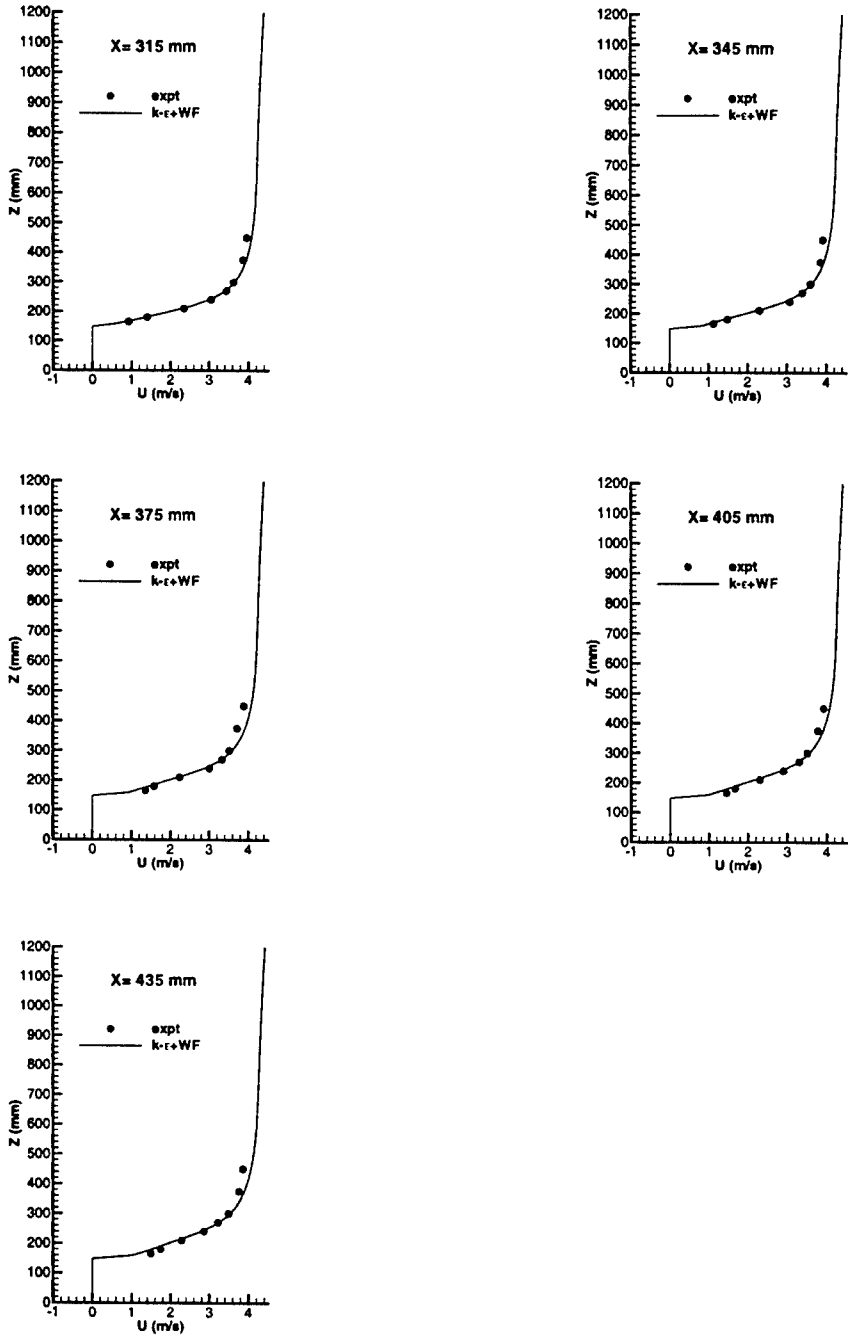

Figure 6. *Vertical profiles of the mean streamwise velocity U at specified x-locations over the roof (2.1 <= x/H <= 2.9) of the second building compared with time-averaged wind tunnel measurements.*

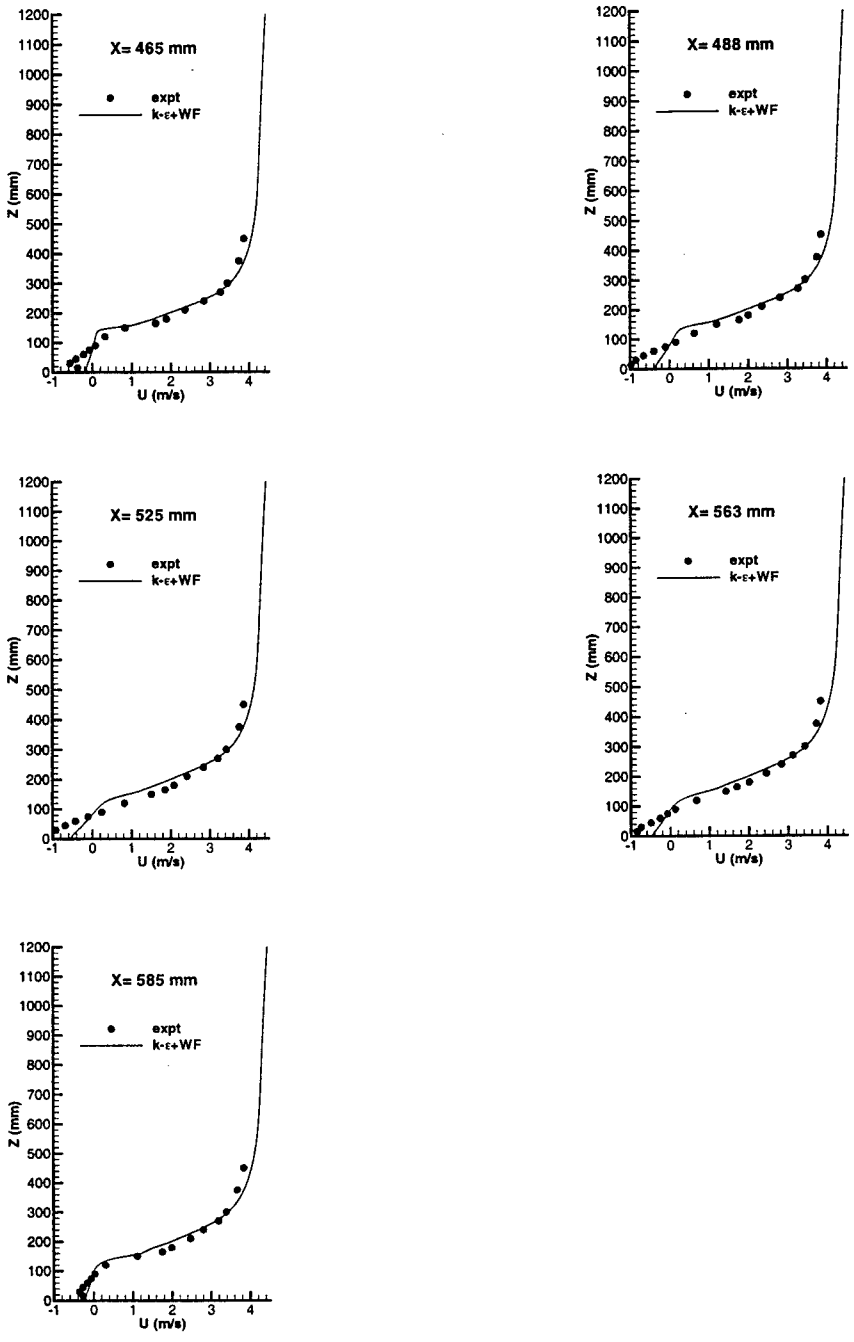

Figure 7. *Vertical profiles of the mean streamwise velocity U at specified x-locations within the second urban canyon* (3.1 <= *x/H* <= 3.9) *compared with time-averaged wind tunnel measurements.*

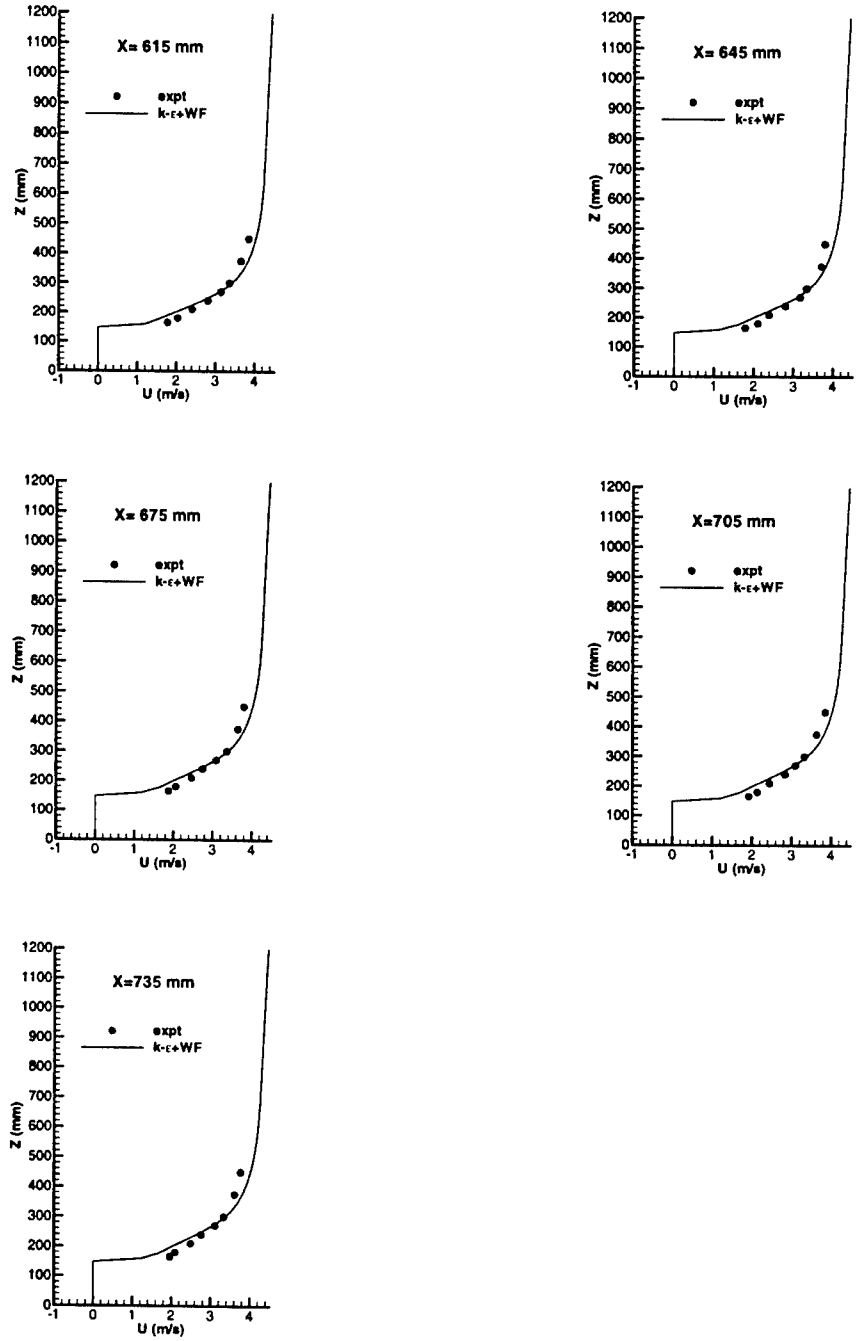

Figure 8. *Vertical profiles of the mean streamwise velocity U at specified x-locations over the roof* (4.1 <= *x/H* <= 4.9) *of the third building compared with time-averaged wind tunnel measurements.*

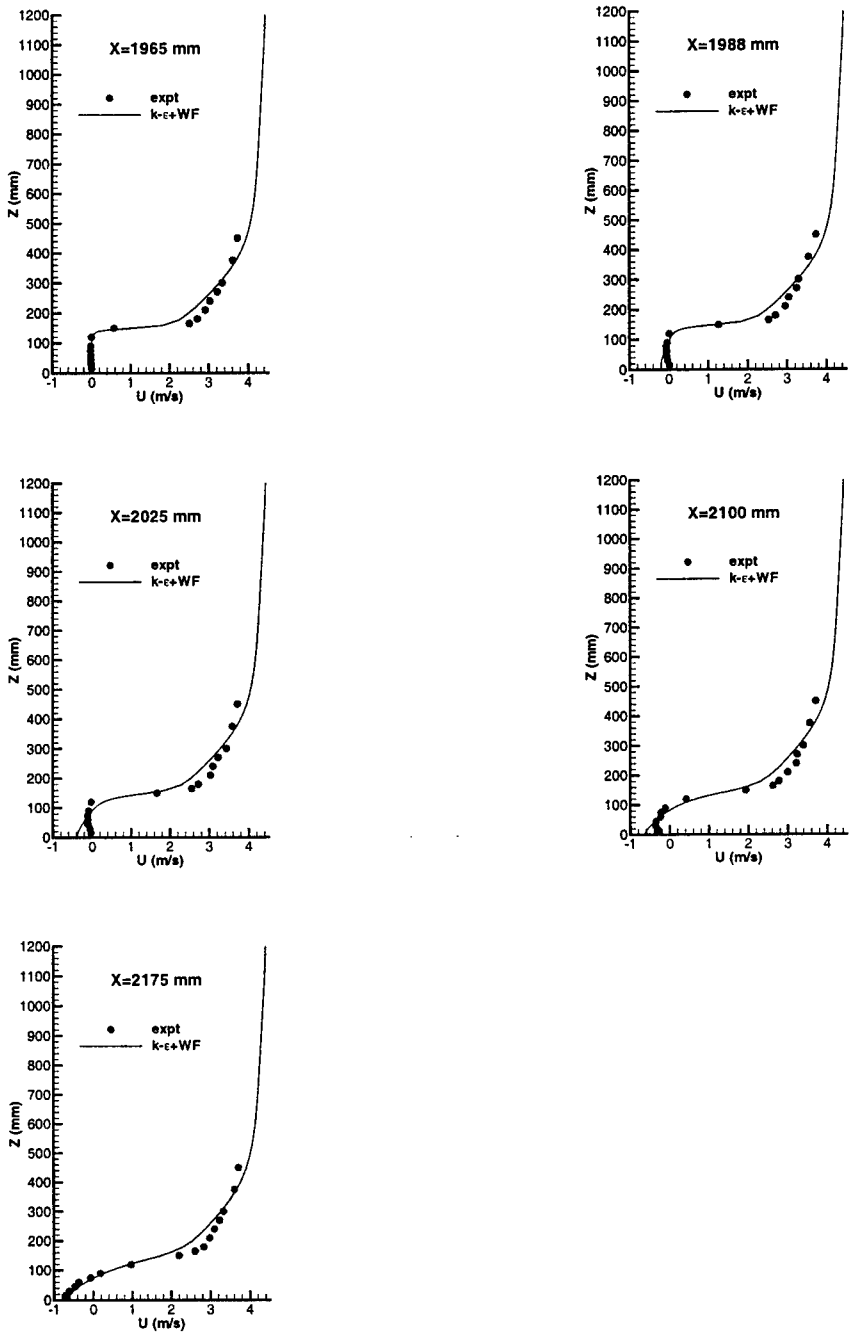

Figure 9. *Vertical profiles of the mean streamwise velocity U at specified x-locations in the exit region* (13.1 <= *x/H* <= 14.5) *downstream of the back face of the last building compared with time-averaged wind tunnel measurements.*

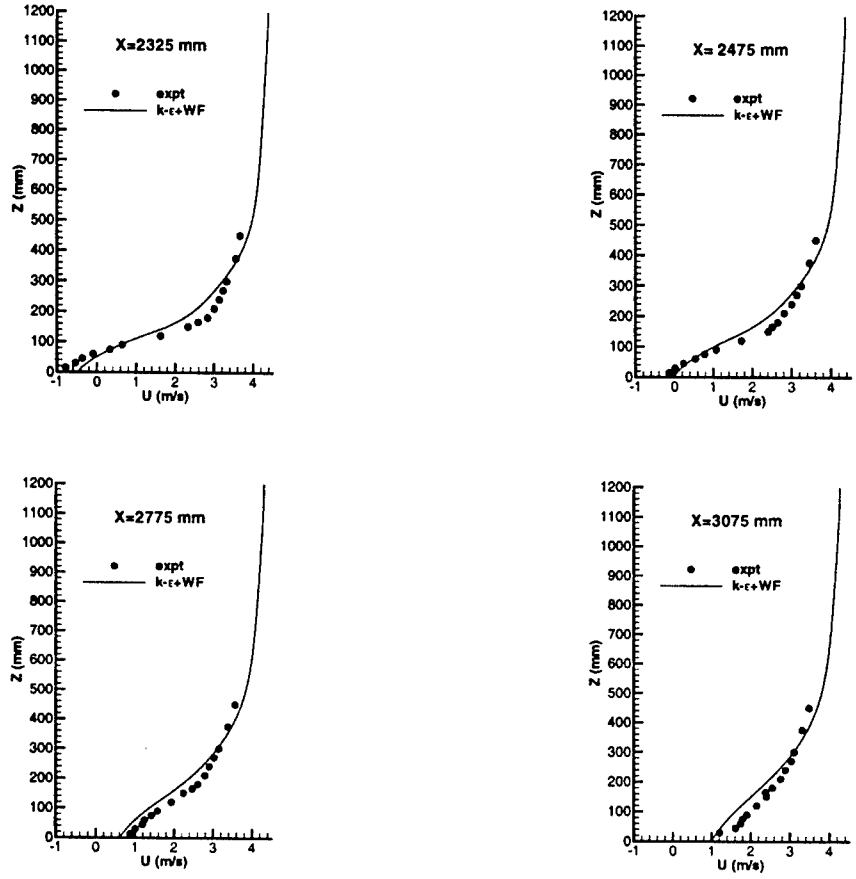

Figure 10. *Vertical profiles of the mean streamwise velocity U at specified x-locations in the exit region* (15.5 <= *x/H* <= 20.5) *downstream of the back face of the last building compared with time-averaged wind tunnel measurements.*

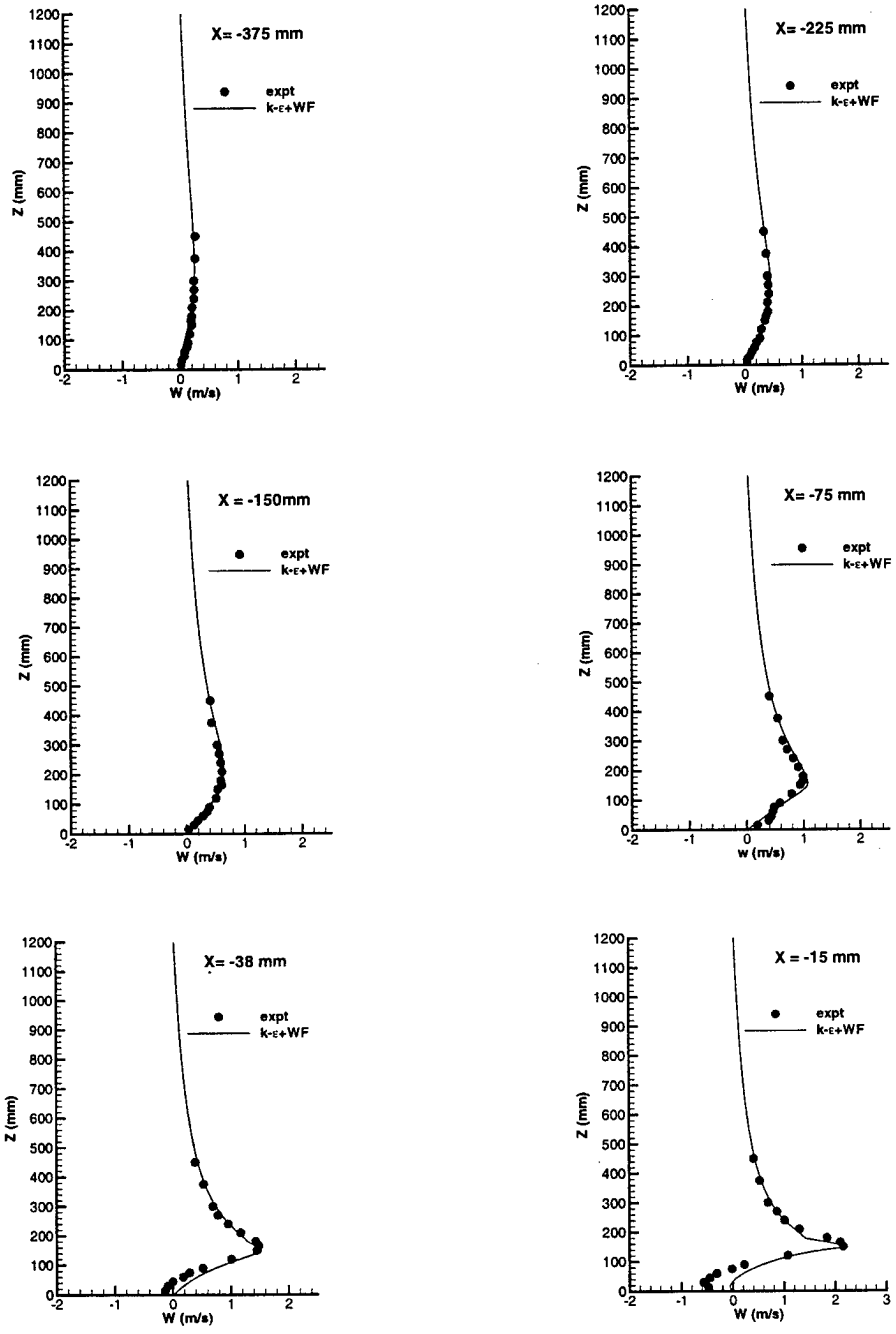

Figure 11. *Vertical profiles of the mean vertical velocity W at specified x-locations in the impingement zone (-2.5 <= x/H <= -0.1) upstream of the front face of the first building compared with time-averaged wind tunnel measurements.*

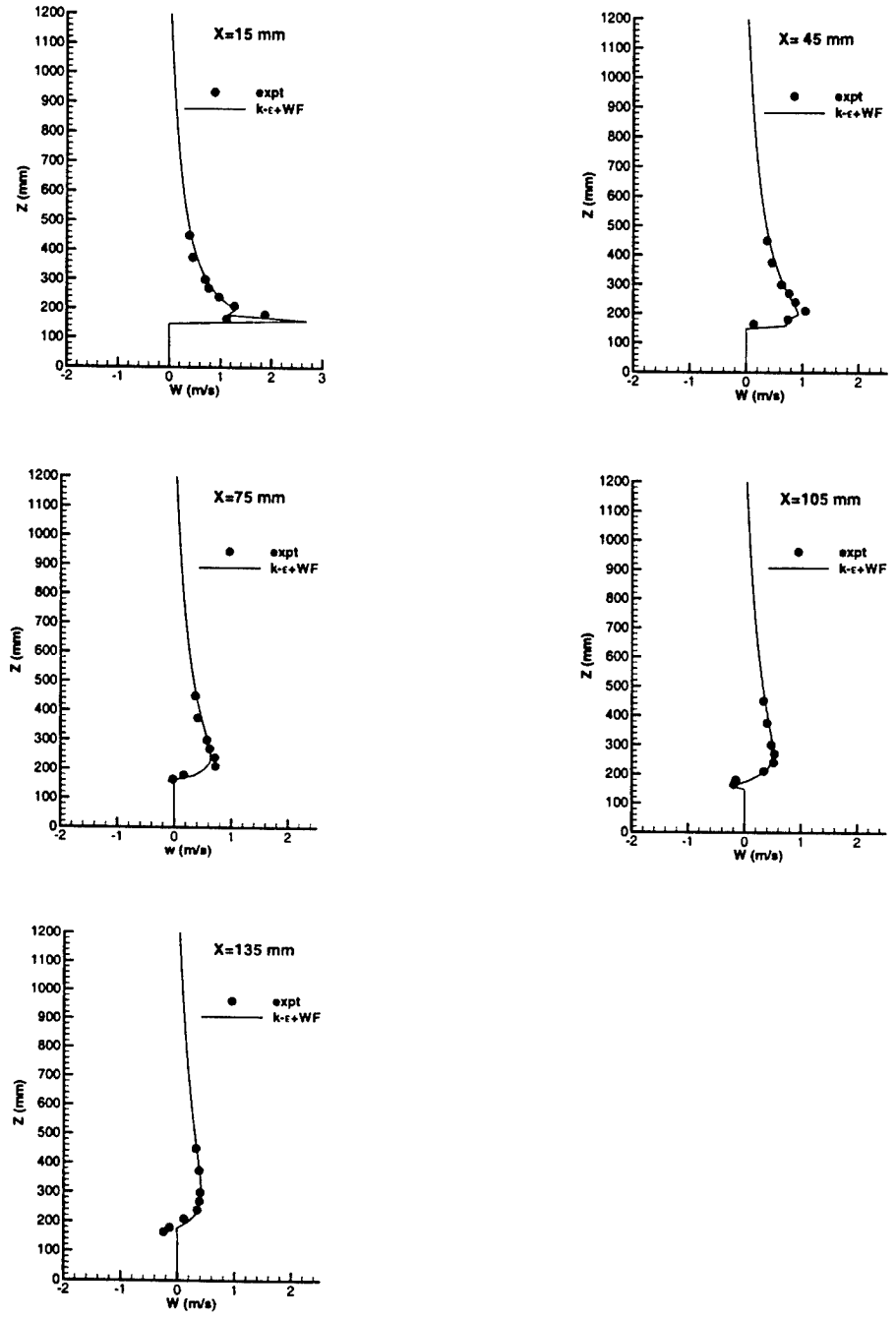

Figure 12. *Vertical profiles of the mean vertical velocity W at specified x-locations over the roof* (0.1<= *x*/*H* <= 0.9) *of the first building compared with time-averaged wind tunnel measurements.*

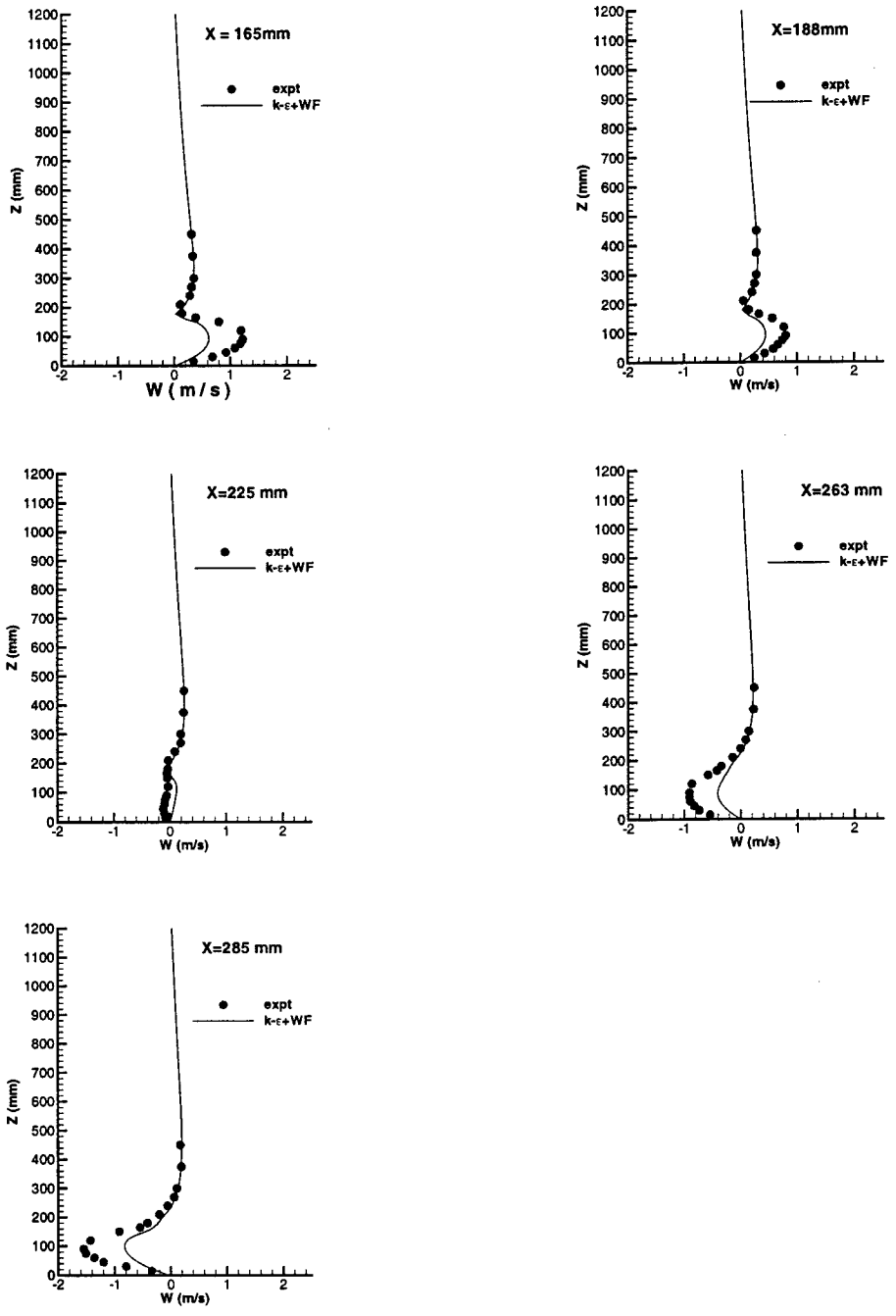

Figure 13. *Vertical profiles of the mean vertical velocity W at specified x-locations within the first urban canyon* (1.1 <= *x/H* <= 1.9) *compared with time-averaged wind tunnel measurements.*

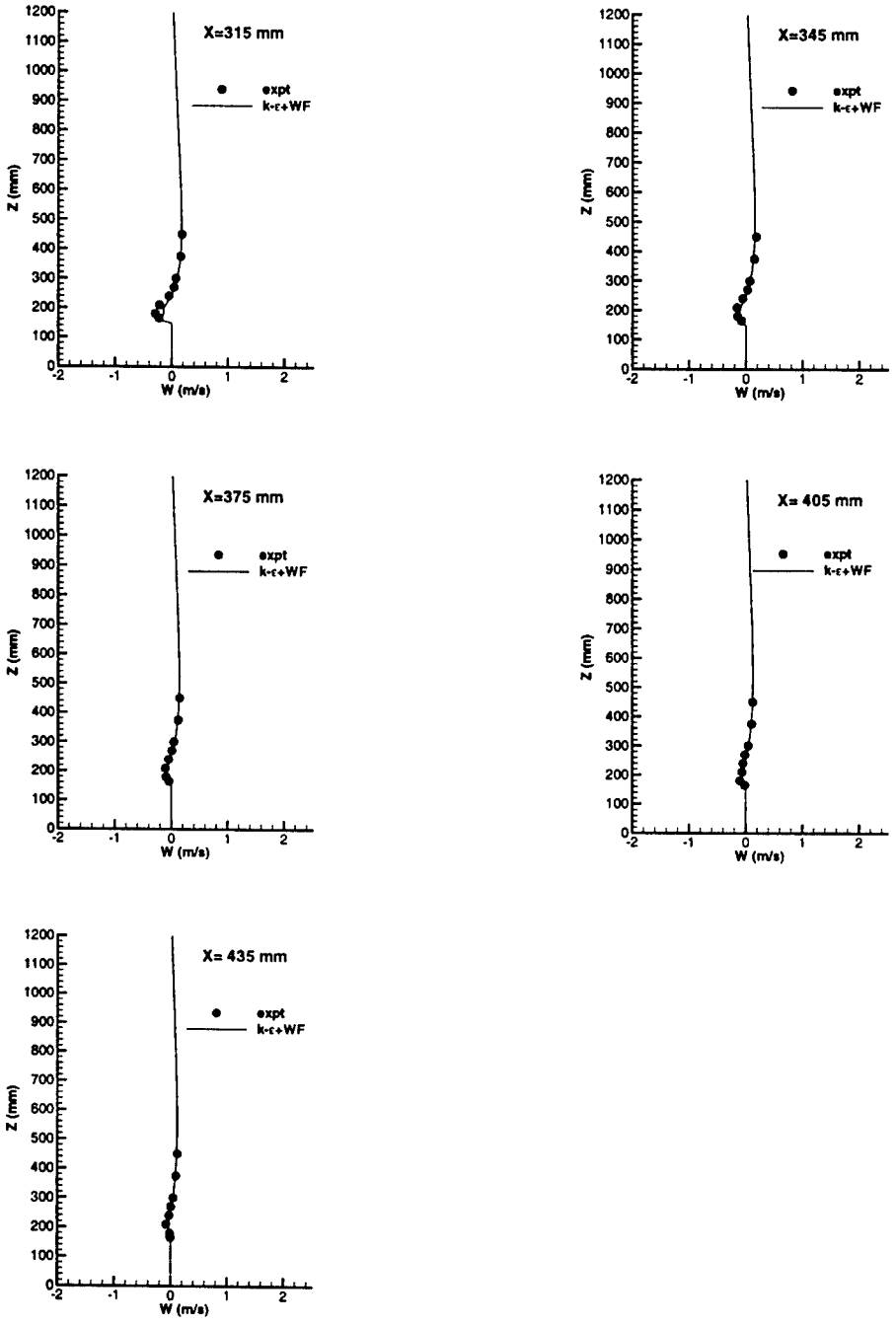

Figure 14. *Vertical profiles of the mean vertical velocity W at specified x-locations over the roof (2.1 <= x/H <= 2.9) of the second building compared with time-averaged wind tunnel measurements.*

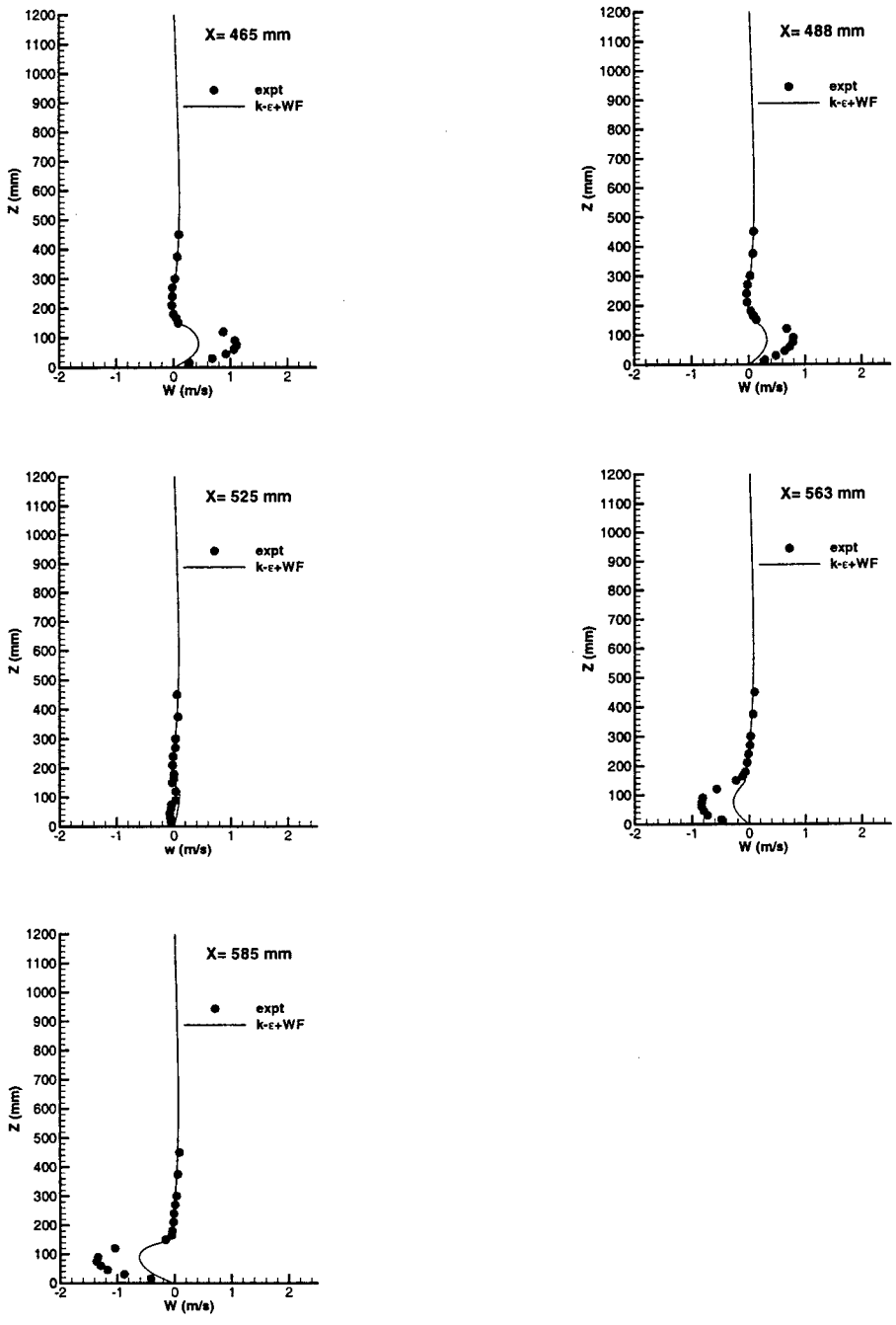

Figure 15. *Vertical profiles of the mean vertical velocity W at specified x-locations within the second urban canyon* (3.1 <= *x/H* <= 3.9) *compared with time-averaged wind tunnel measurements.*

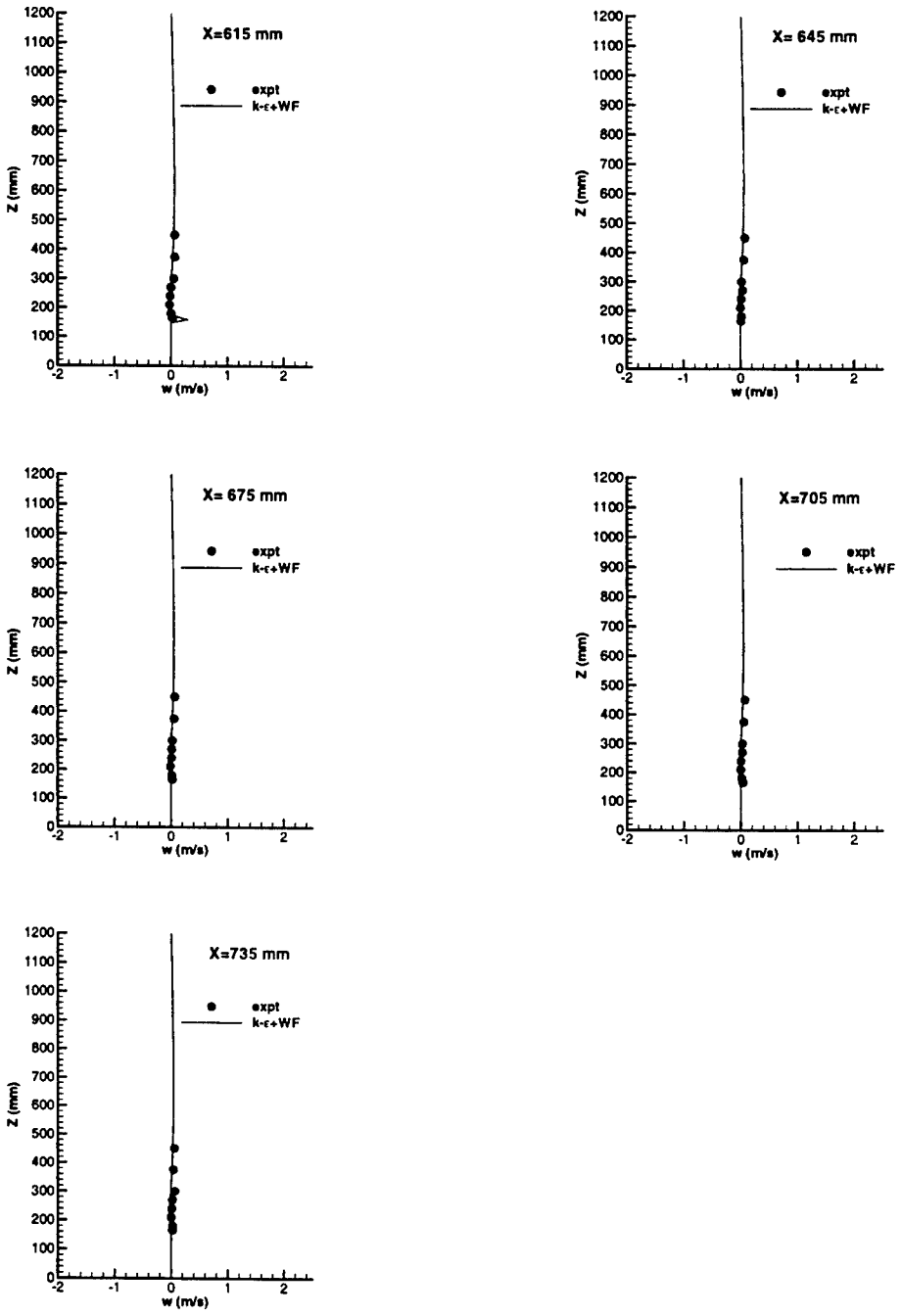

Figure 16. *Vertical profiles of the mean vertical velocity W at specified x-locations over the roof* (4.1 <= *x/H* <= 4.9) *of the third building compared with time-averaged wind tunnel measurements.*

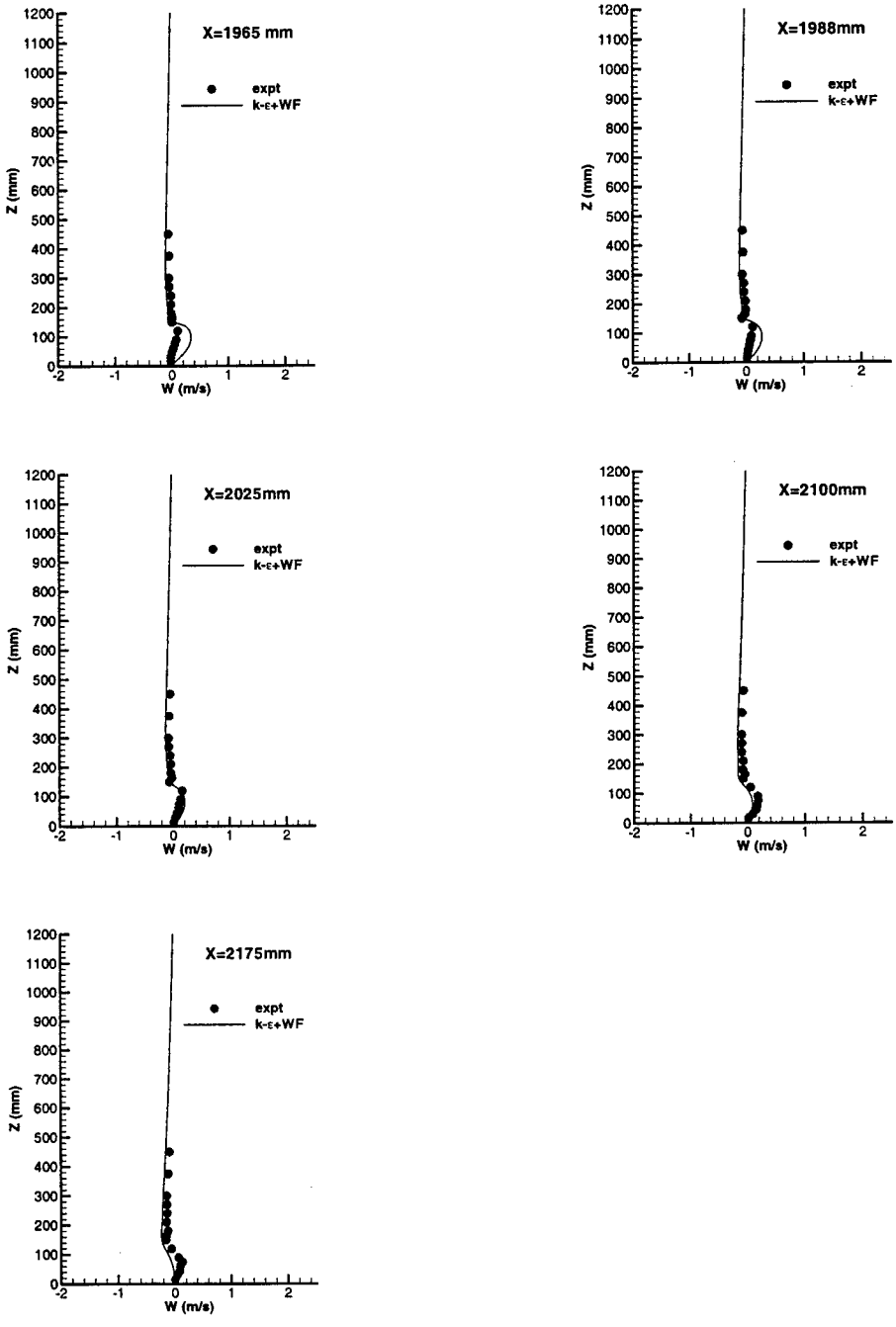

Figure 17. *Vertical profiles of the mean vertical velocity W at specified x-locations in the exit region* (13.1 <= *x/H* <= 14.5) *downstream of the back face of the last building compared with time-averaged wind tunnel measurements.*

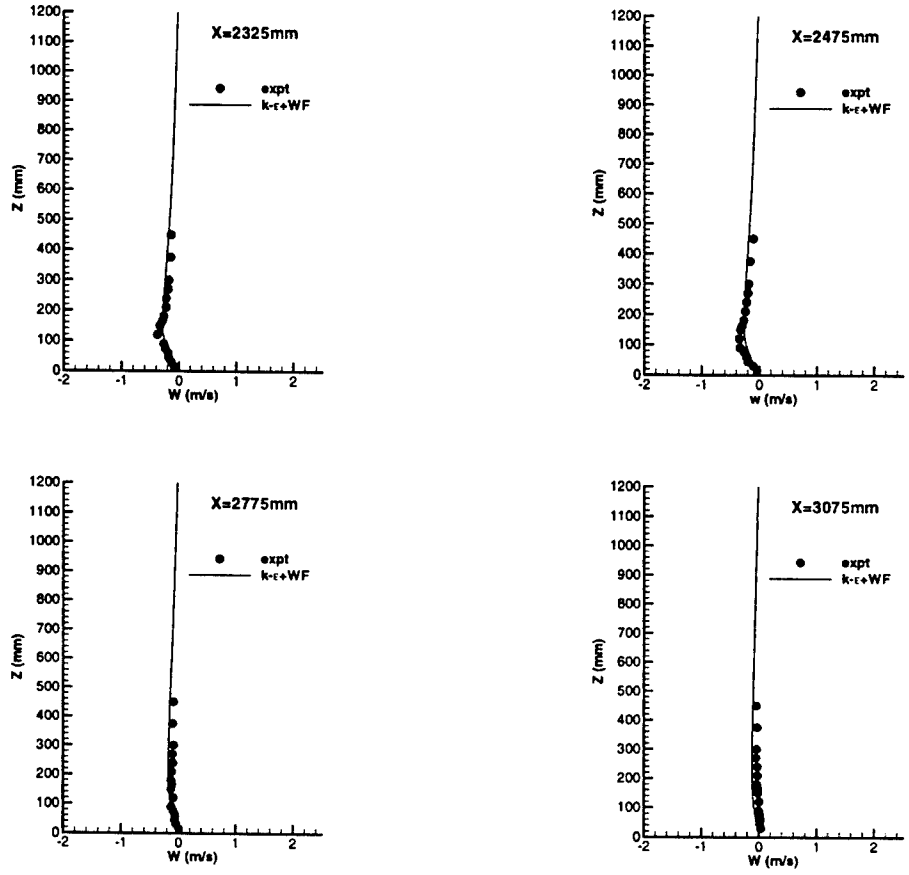

Figure 18. *Vertical profiles of the mean vertical velocity W at specified x-locations in the exit region* (15.5 <= *x/H* <= 20.5) *downstream of the back face of the last building compared with time-averaged wind tunnel measurements.*

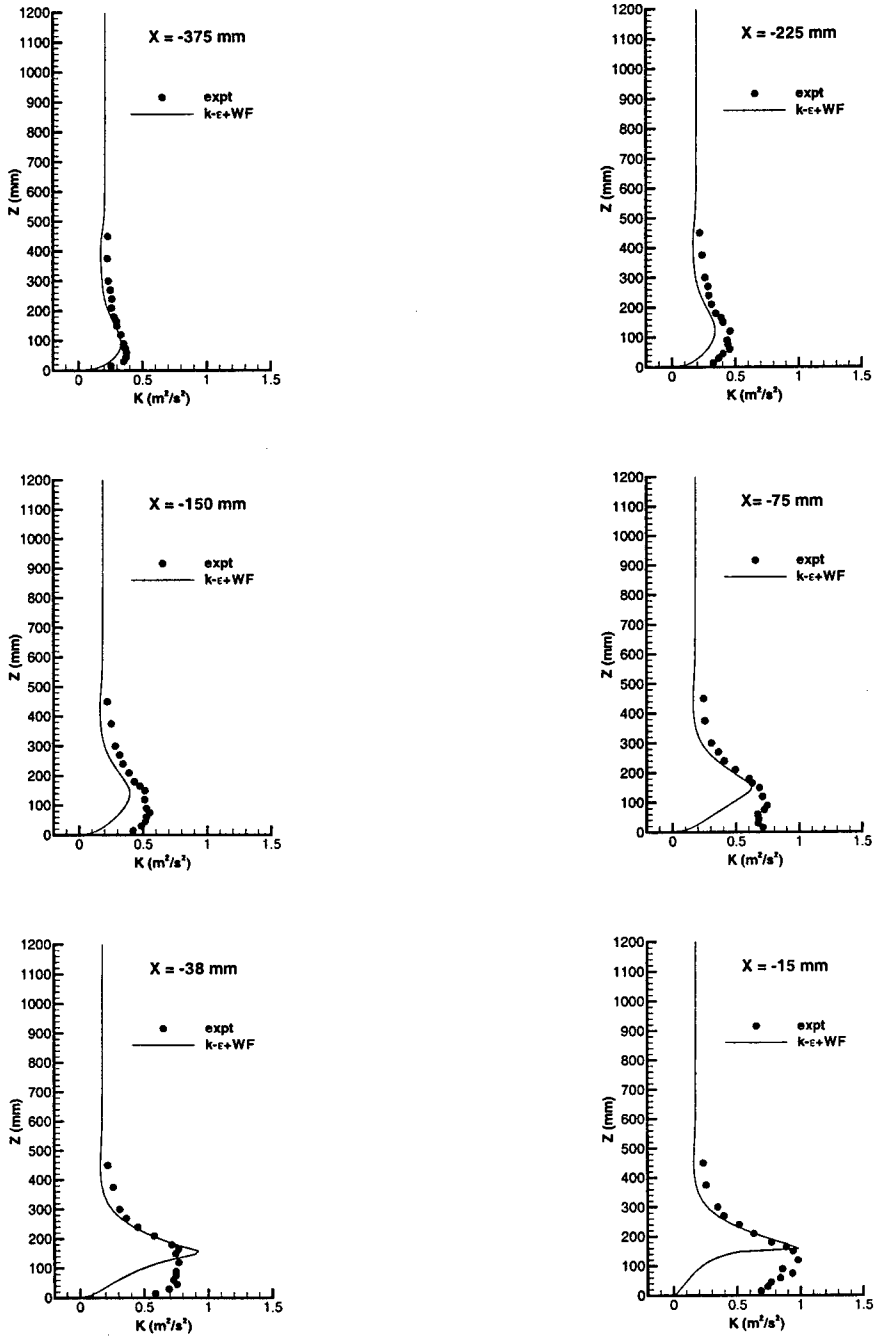

Figure 19. *Vertical profiles of the turbulence kinetic energy k at specified x-locations in the impingement zone* (-2.5 <= *x/H* <= -0.1) *upstream of the front face of the first building compared with time-averaged wind tunnel measurements.*

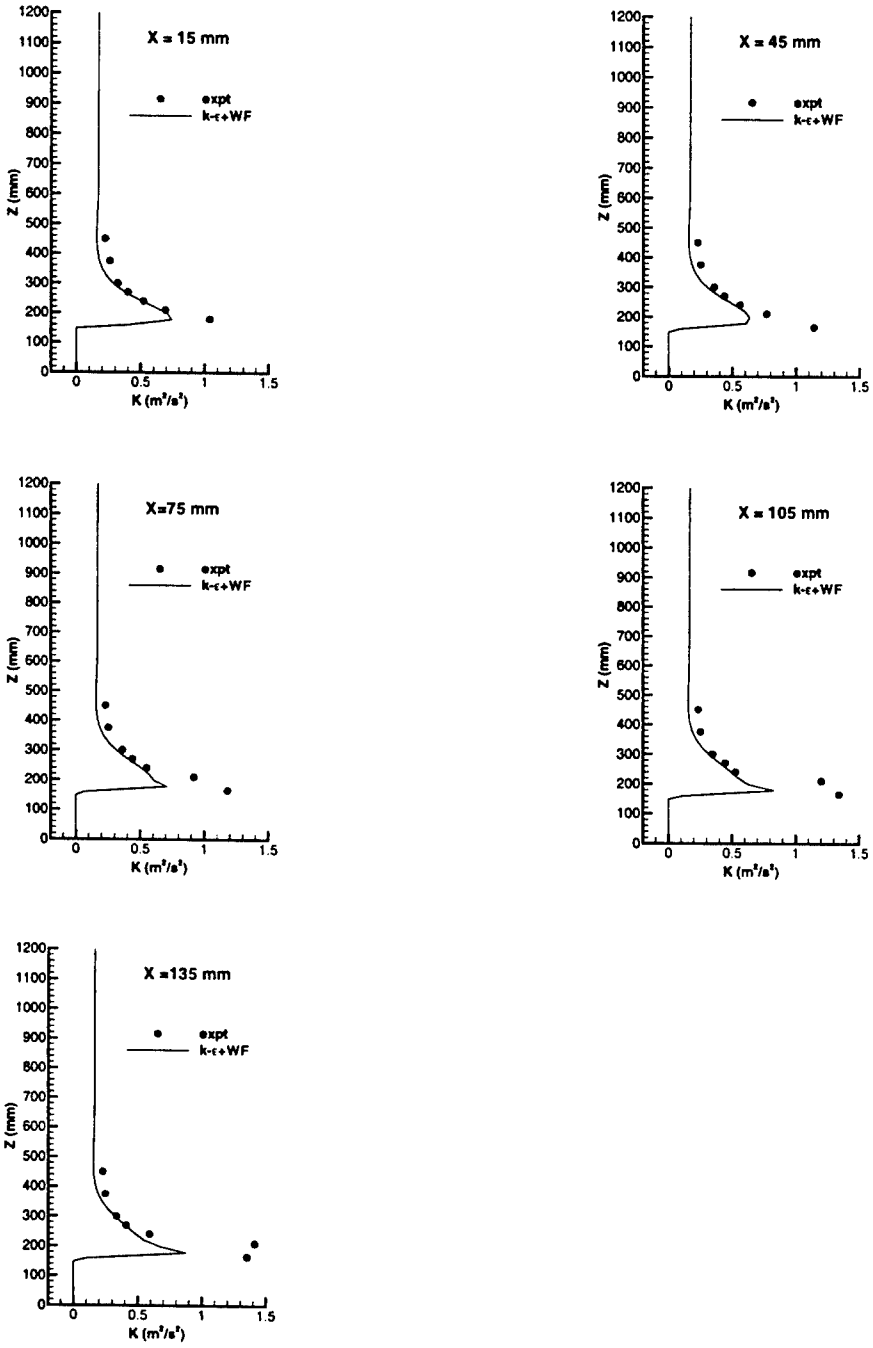

Figure 20. *Vertical profiles of the turbulence kinetic energy k at specified x-locations over the roof* (0.1 <= *x/H* <= 0.9) *of the first building compared with time-averaged wind tunnel measurements.*

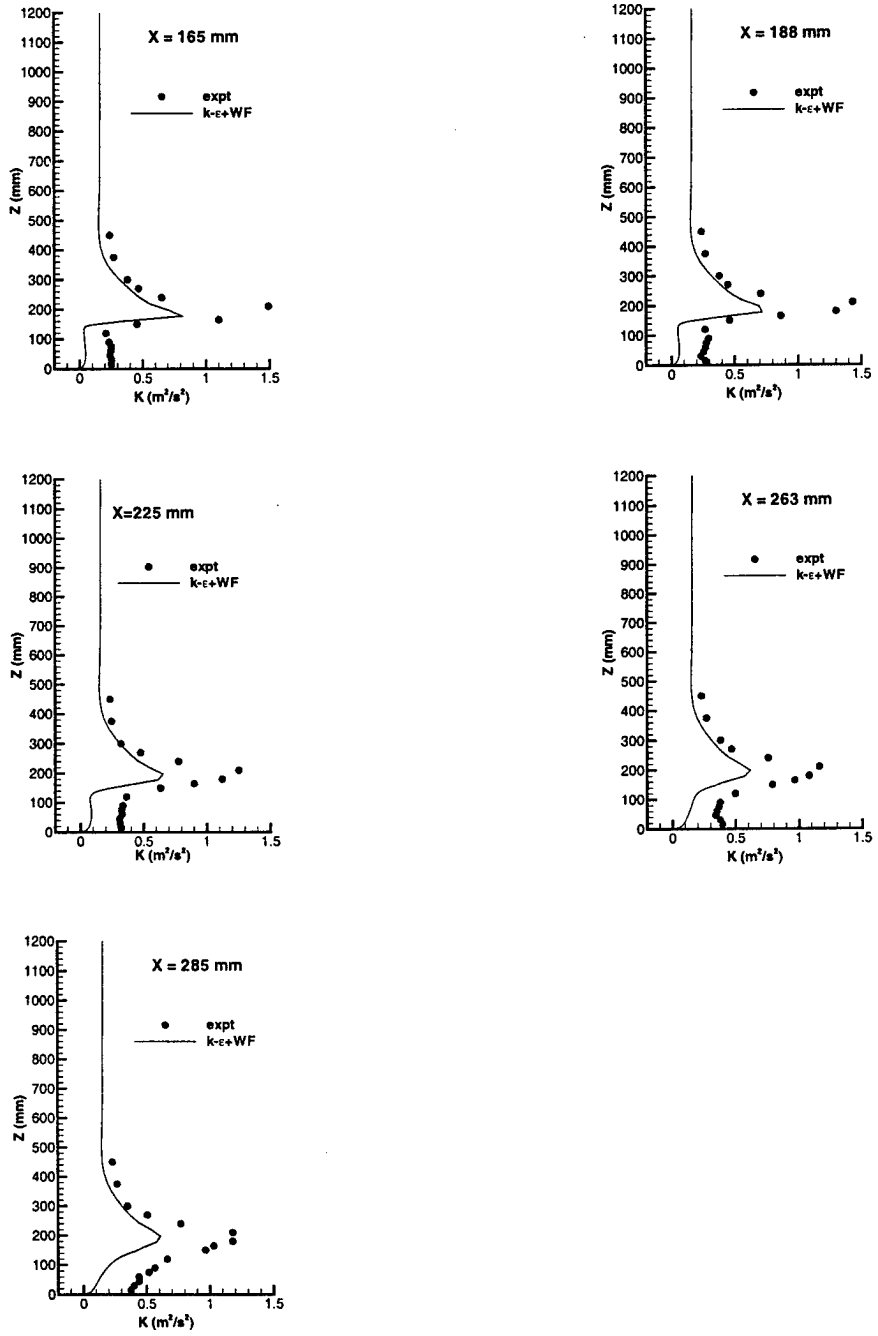

Figure 21. *Vertical profiles of the turbulence kinetic energy k at specified x-locations within the first urban canyon* (1.1 <= *x/H* <= 1.9) *compared with time-averaged wind tunnel measurements.*

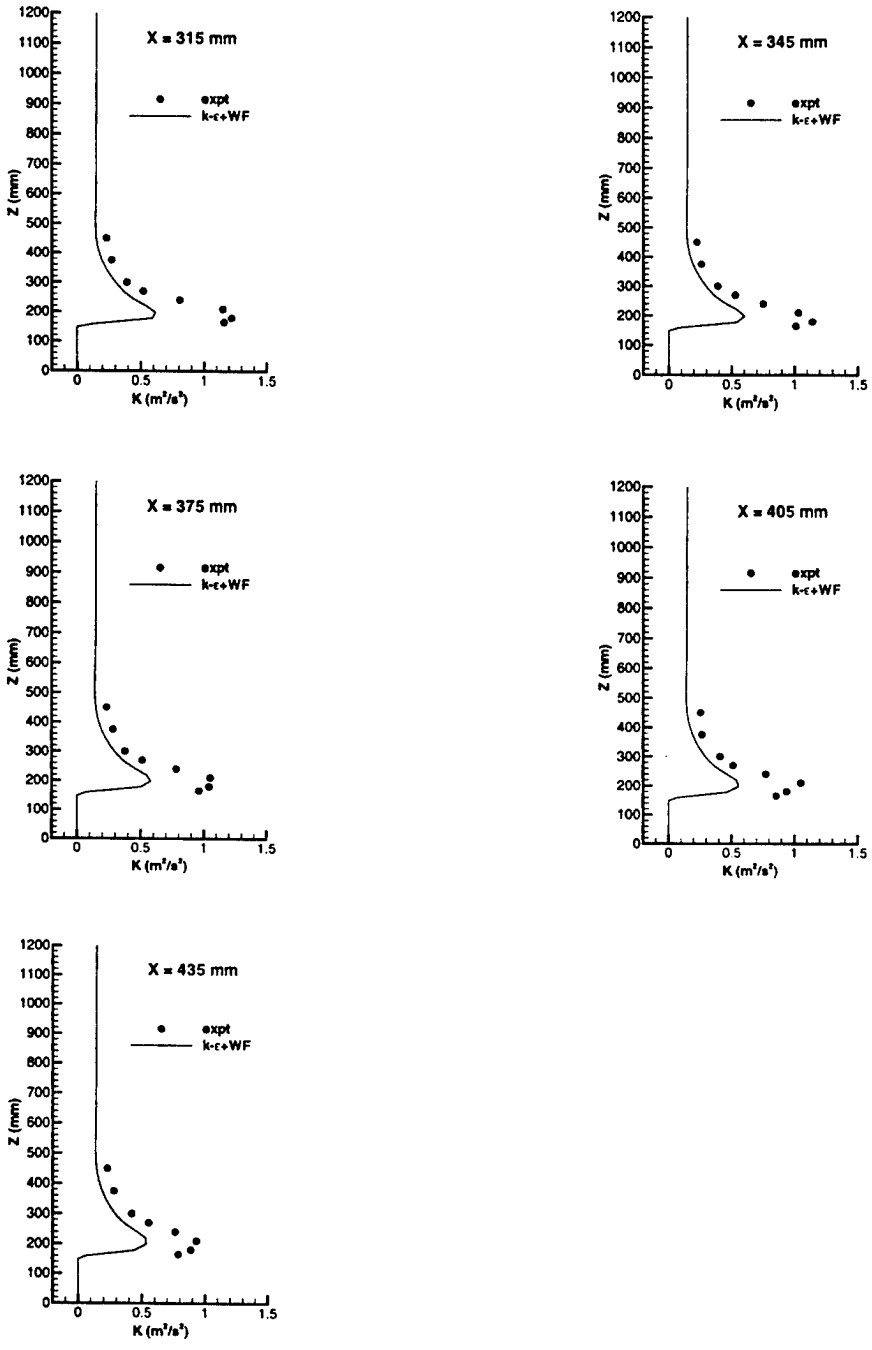

Figure 22. *Vertical profiles of the turbulence kinetic energy at specified x-locations over the roof (2.1 <= x/H <= 2.9) of the second building compared with time-averaged wind tunnel measurements.*

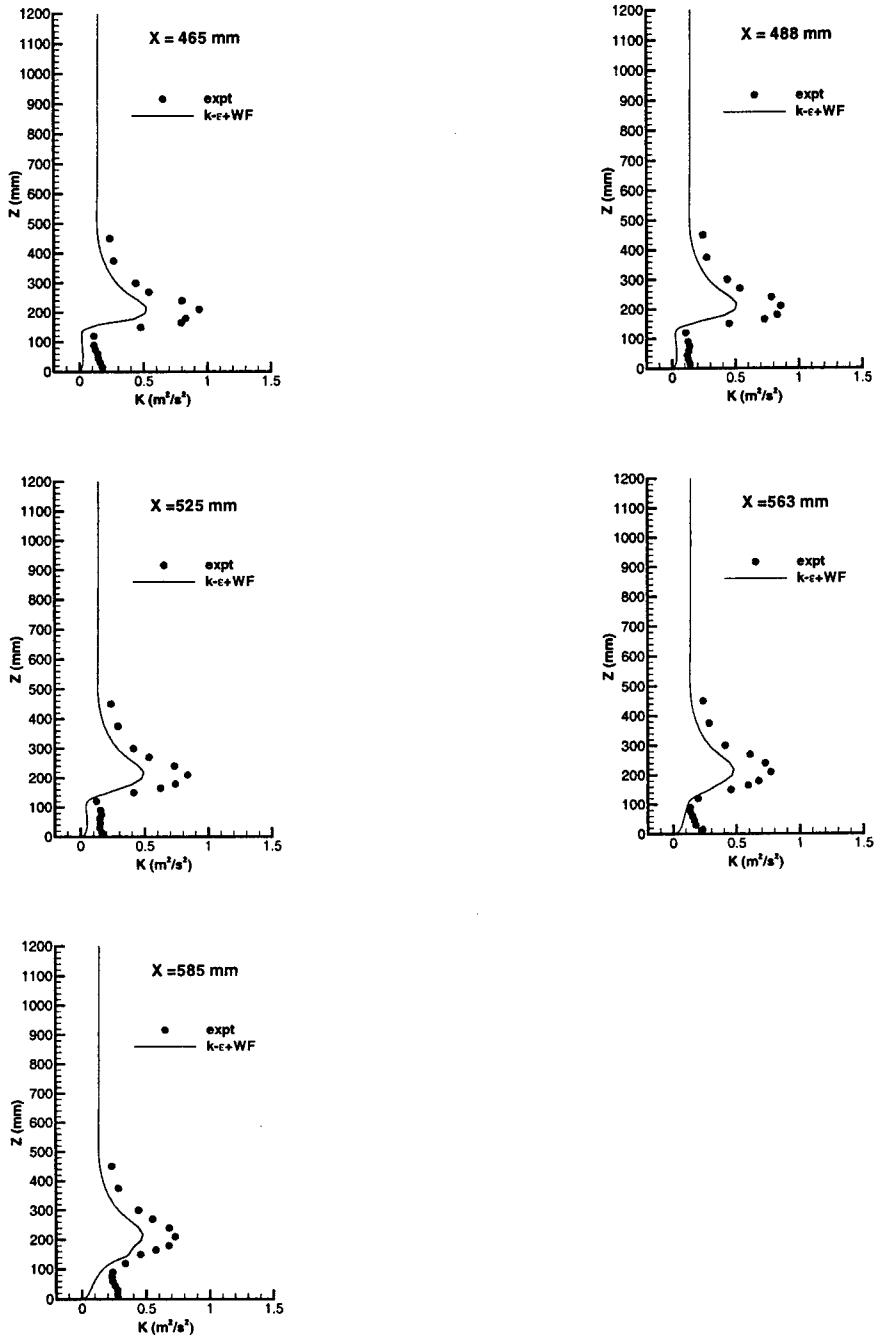

Figure 23. *Vertical profiles of the turbulence kinetic energy k at specified x-locations within the second urban canyon* (3.1 <= *x/H* <= 3.9) *compared with time-averaged wind tunnel measurements.*

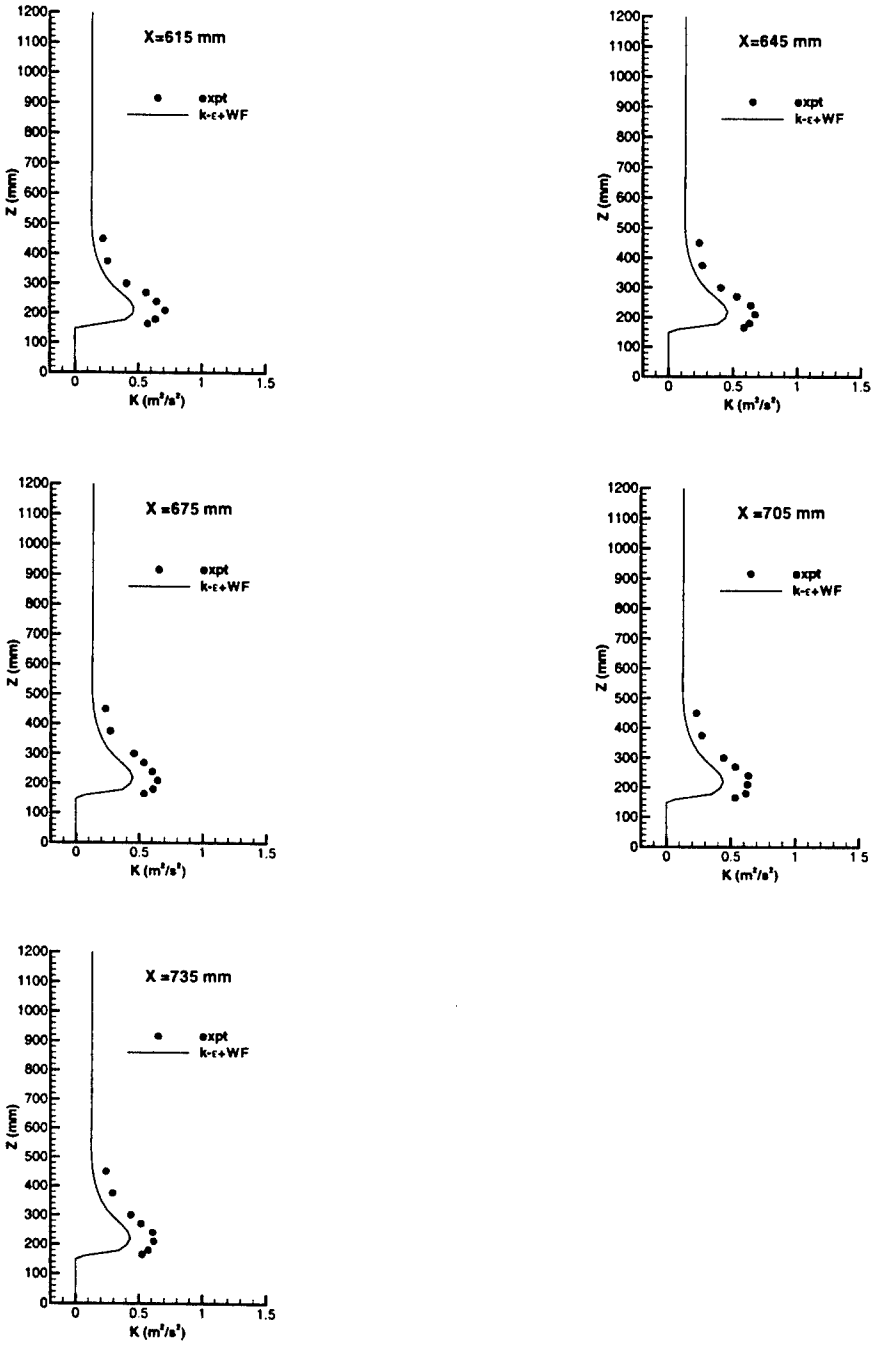

Figure 24. *Vertical profiles of the turbulence kinetic energy k at specified x-locations over the roof (4.1 <= x/H <= 4.9) of the third building compared with time-averaged wind tunnel measurements.*

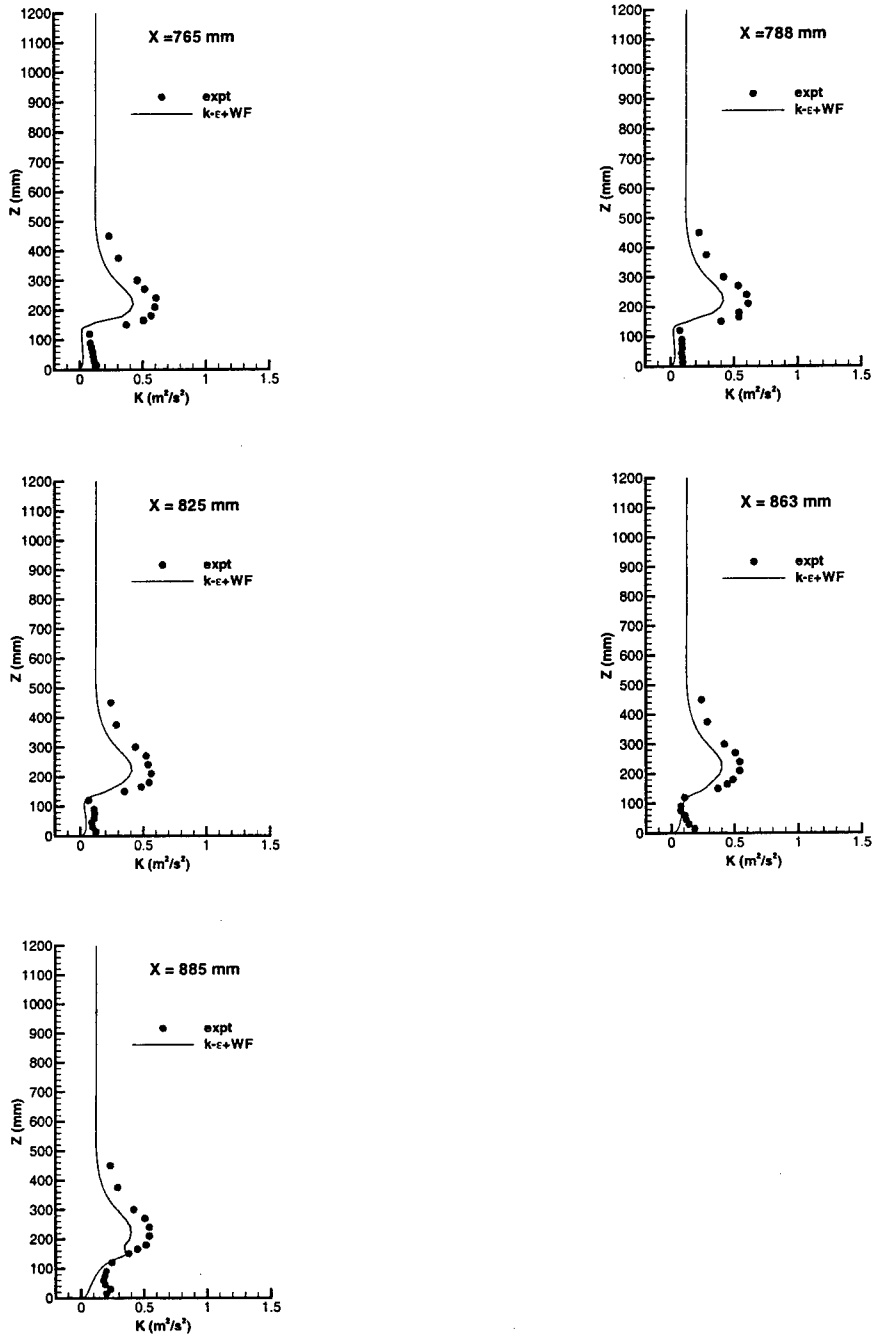

Figure 25. *Vertical profiles of the turbulence kinetic energy k at specified x-locations within the third urban canyon* (5.1 <= *x/H* <= 5.9) *compared with time-averaged wind tunnel measurements*

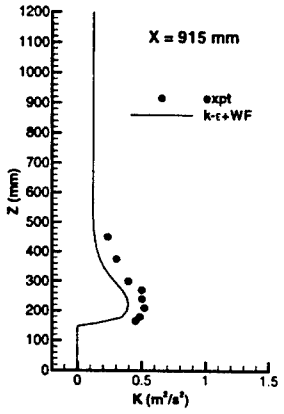

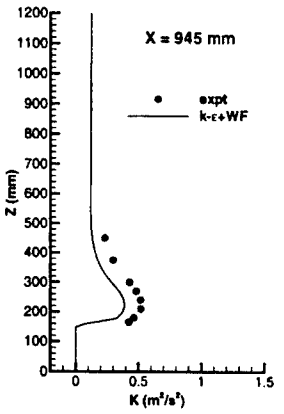

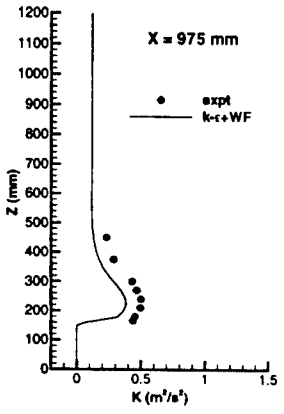

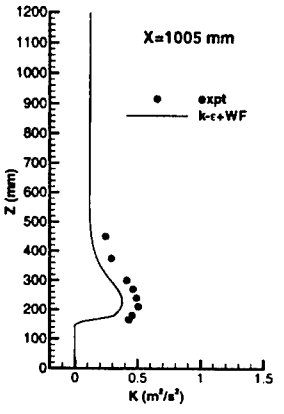

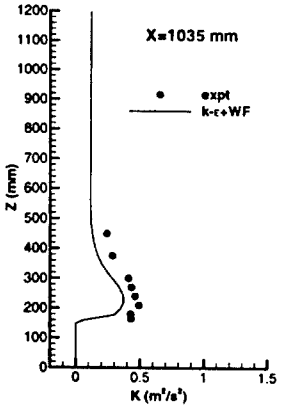

Figure 26. *Vertical profiles of the turbulence kinetic energy k at specified x-locations over the roof* (6.1 <= *x/H* <= 6.9) *of the fourth building compared with time-averaged wind tunnel measurements.*

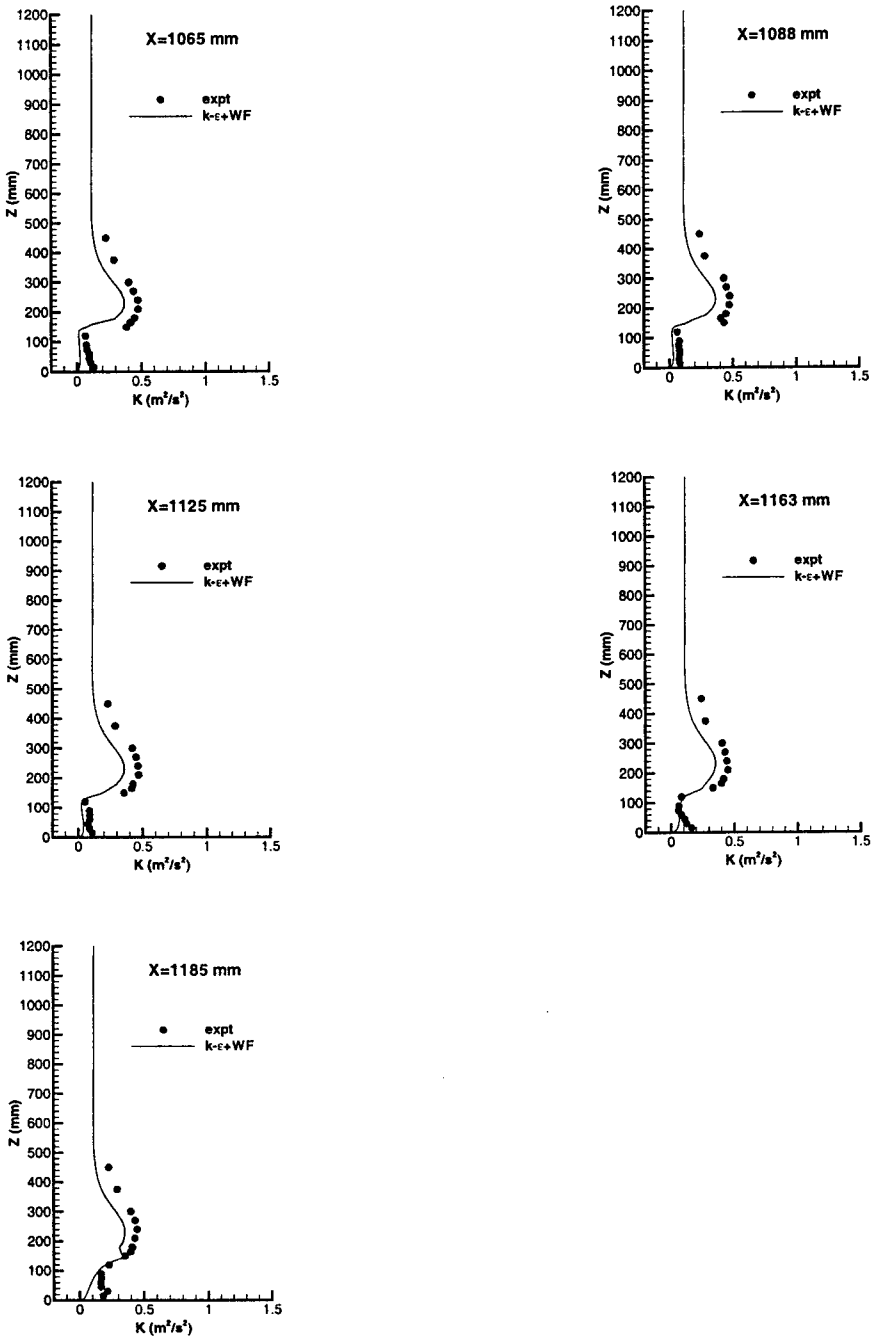

Figure 27. *Vertical profiles of the turbulence kinetic energy k at specified x-locations within the fourth urban canyon* (7.1 <= *x/H* <= 7.9) *compared with time-averaged wind tunnel measurements.*

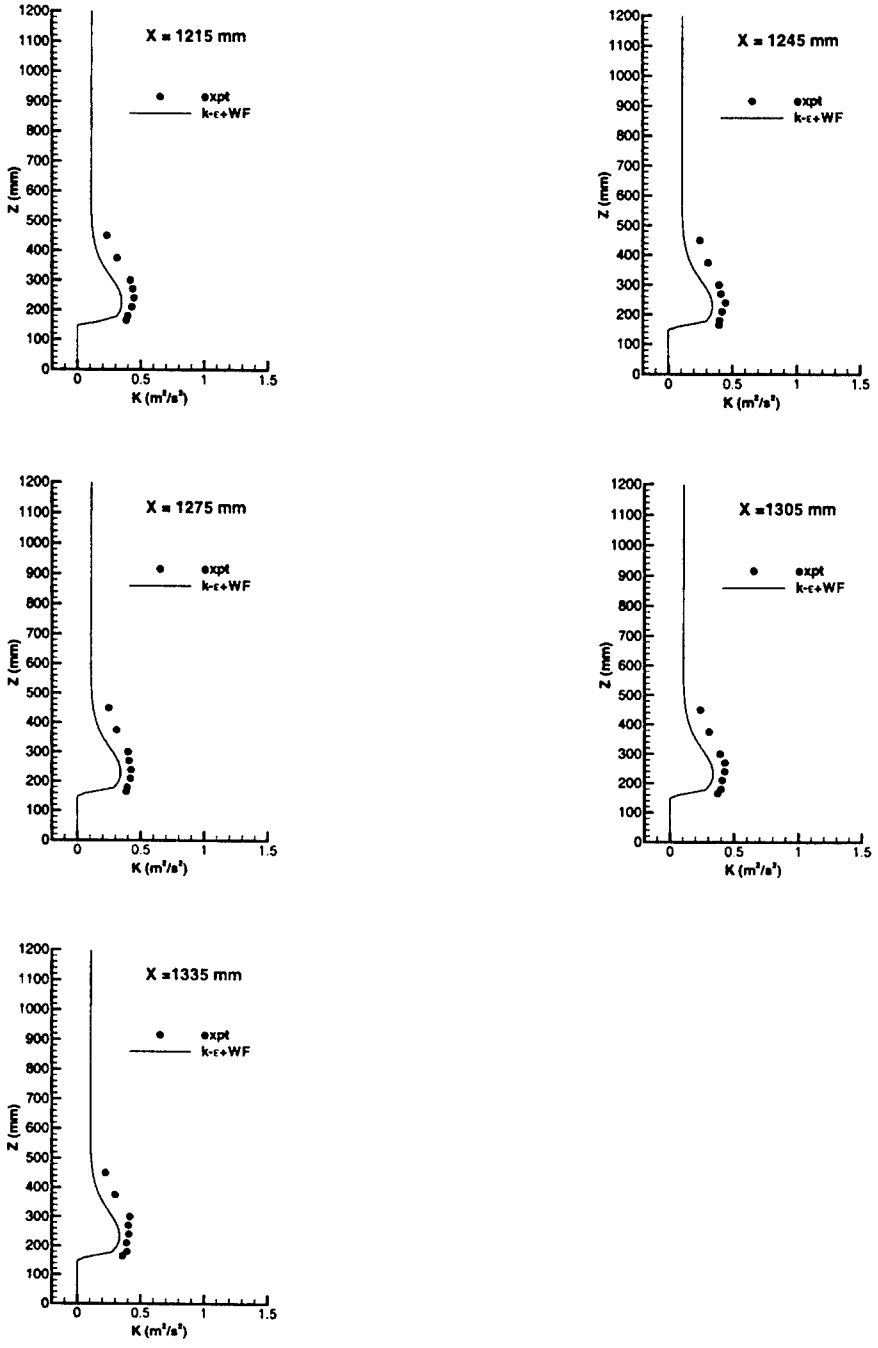

Figure 28. *Vertical profiles of the turbulence kinetic energy k at specified x-locations over the roof* (8.1 <= *x/H* <= 8.9) *of the fifth building compared with time-averaged wind tunnel measurements.*

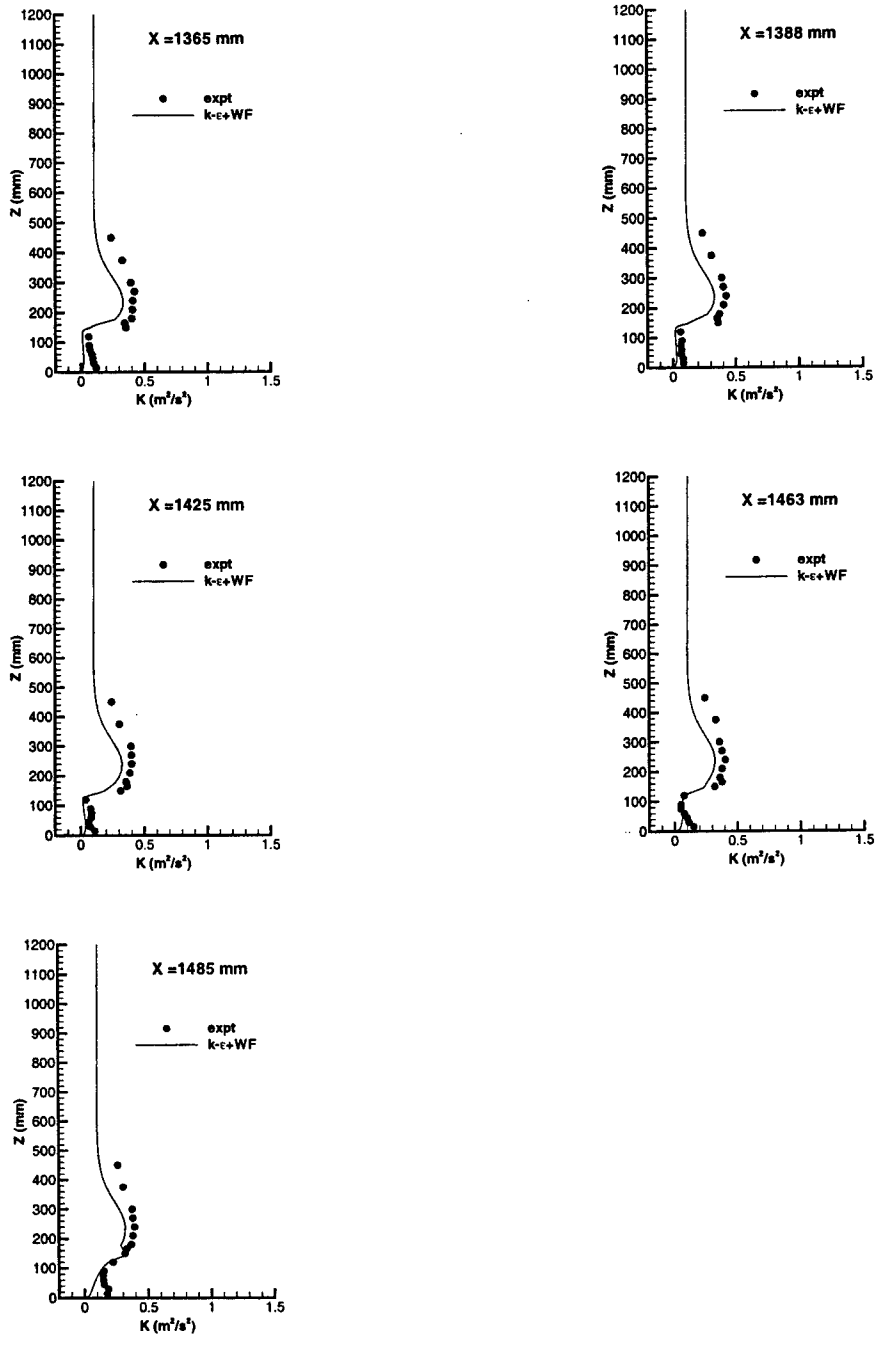

Figure 29. *Vertical profiles of the turbulence kinetic energy k at specified x-locations within the fifth urban canyon* (9.1 <= *x/H* <= 9.9) *compared with time-averaged wind tunnel measurements.*

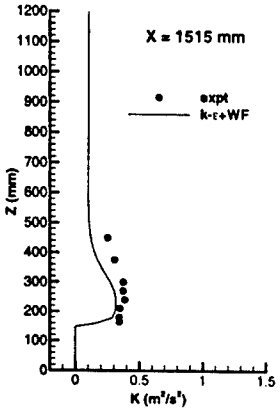

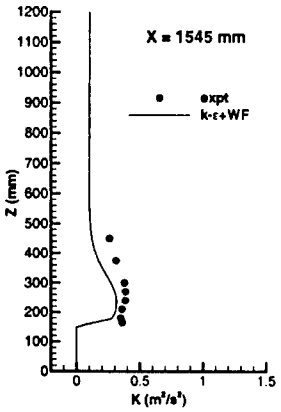

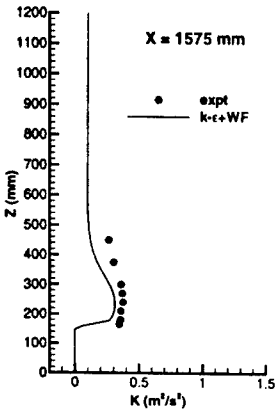

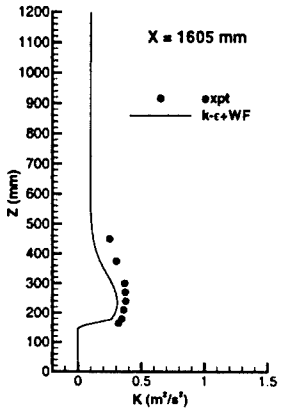

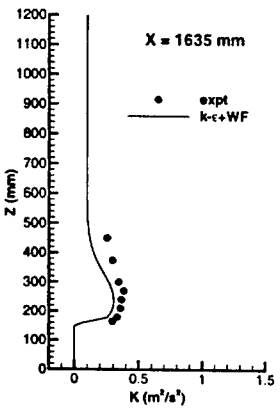

Figure 30. *Vertical profiles of the turbulence kinetic energy k at specified x-locations over the roof* (10.1 <= *x/H* <= 10.9) *of the sixth building compared with time-averaged wind tunnel measurements.*

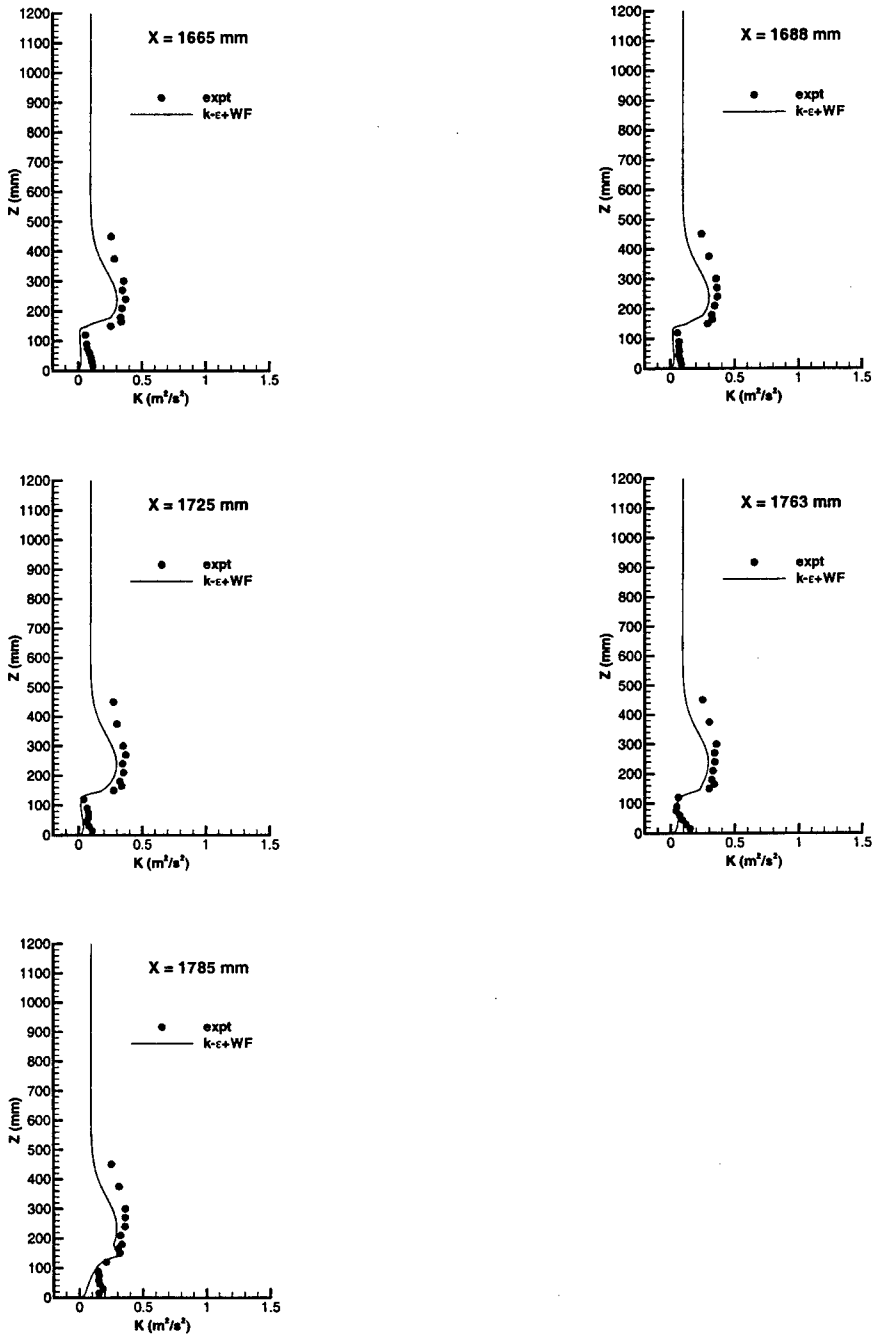

Figure 31. *Vertical profiles of the turbulence kinetic energy k at specified x-locations within the sixth urban canyon* (11.1 <= *x/H* <= 11.9) *compared with time-averaged wind tunnel measurements.*

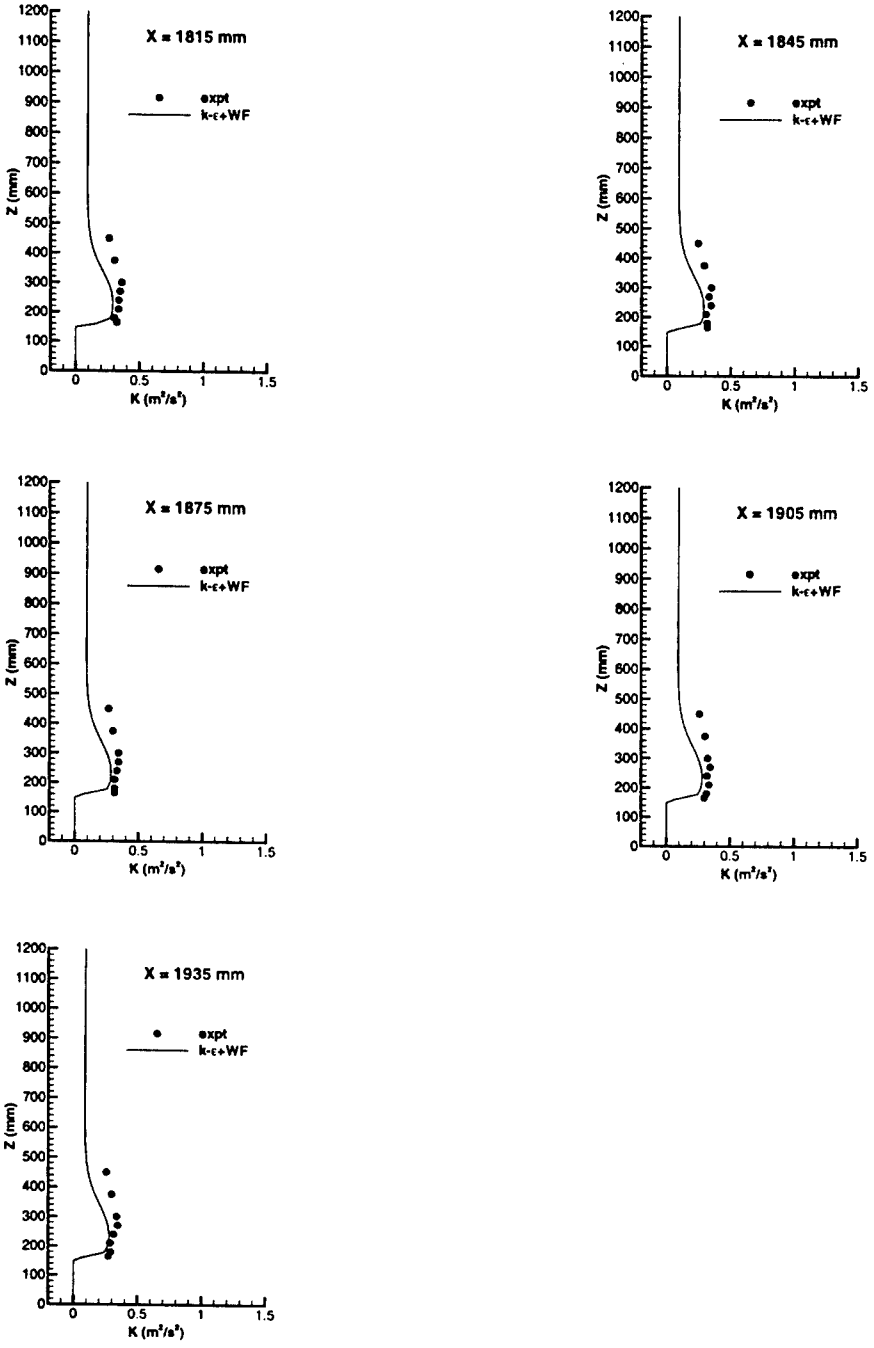

Figure 32. *Vertical profiles of the turbulence kinetic energy k at specified x-locations over the roof* (12.1 <= *x/H* <= 12.9) *of the seventh building compared with time-averaged wind tunnel measurements.*

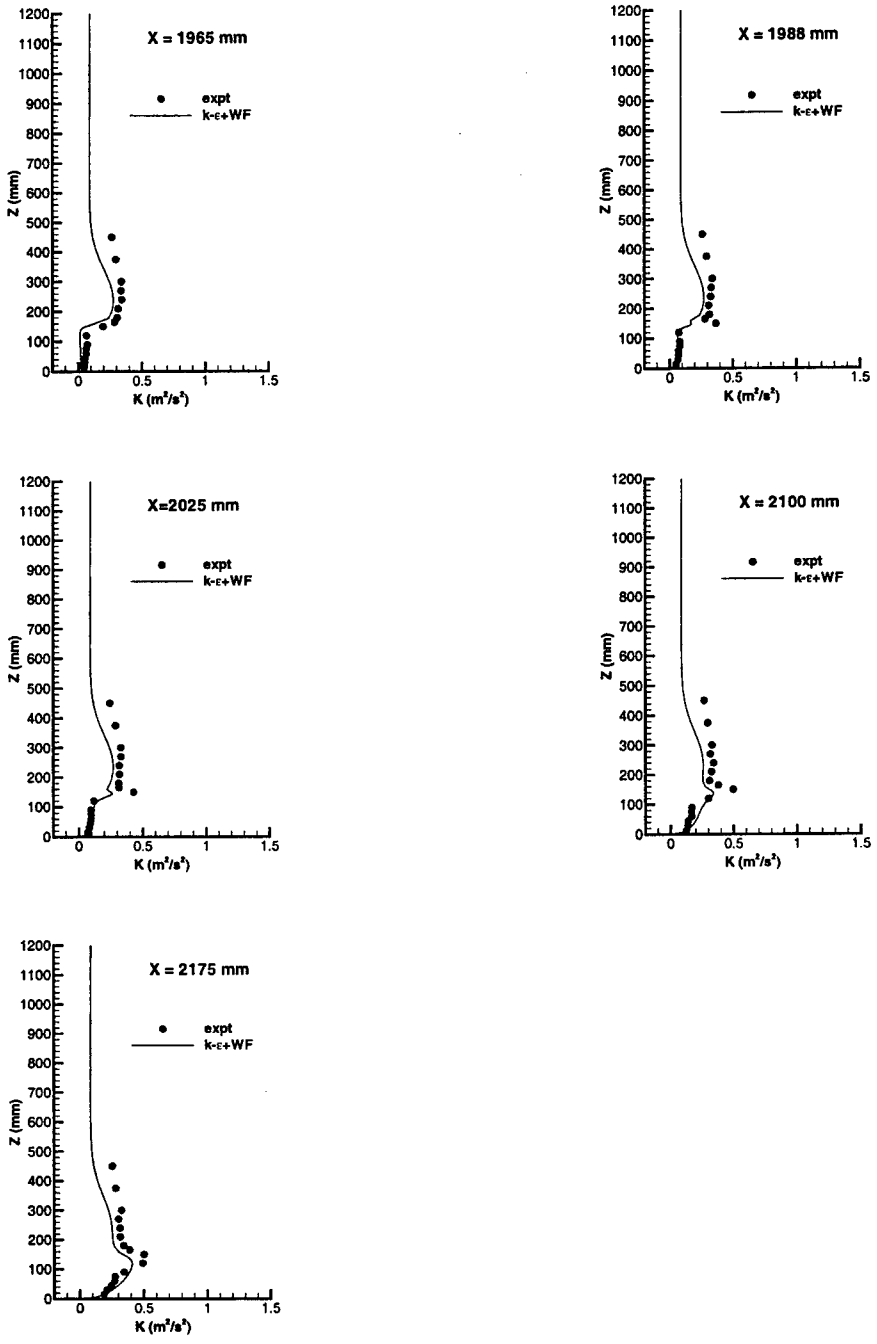

Figure 33. *Vertical profiles of the turbulence kinetic energy k at specified x-locations in the exit region* (13.1 <= *x/H* <= 14.5) *downstream of the back face of the last building compared with time-averaged wind tunnel measurements.*

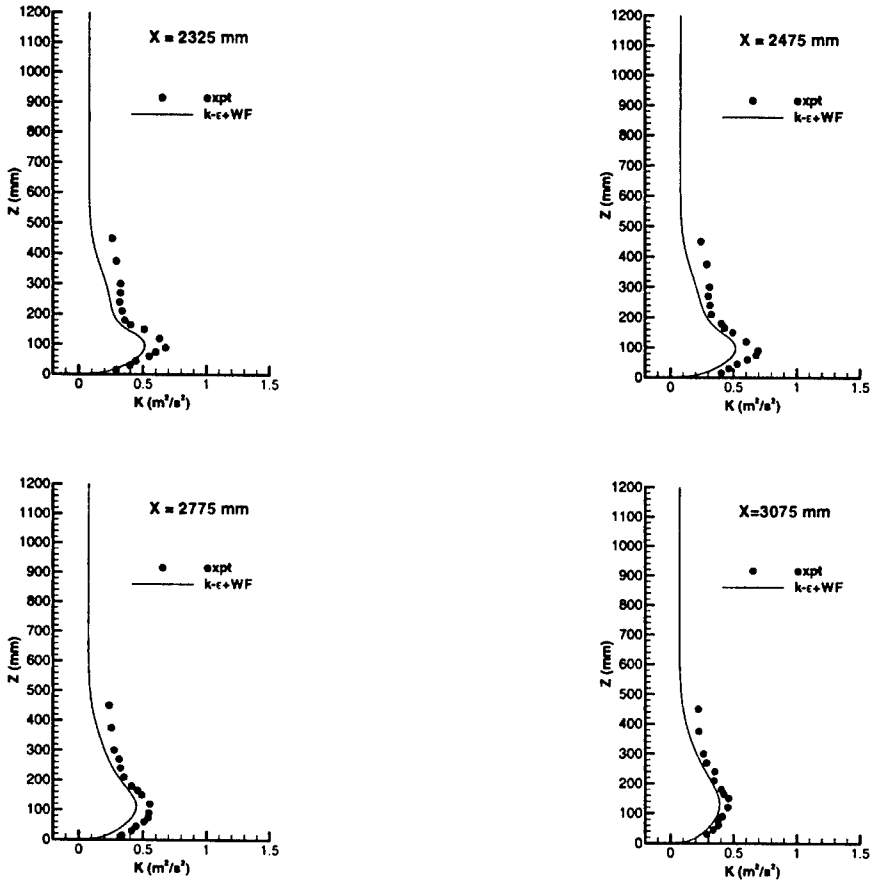

Figure 34. *Vertical profiles of the turbulence kinetic energy k at specified x-locations in the exit region* (15.5 <= *x/H* <= 20.5) *downstream of the back face of the last building compared with time-averaged wind tunnel measurements.*

DOCUMENT CONTROL DATA

(Security classification of title, body of abstract and indexing annotation must be entered when the overall document is classified)

1. ORIGINATOR (the name and address of the organization preparing the document. Organizations for whom the document was prepared, e.g. Establishment sponsoring a contractor's report, or tasking agency, are entered in section 8.)

Defence Research Establishment Suffield
P.O. Box 4000
Medicine Hat, Alberta T1A 8K6

2. SECURITY CLASSIFICATION (overall security classification of the document. including special warning terms if applicable)

UNCLASSIFIED

3. TITLE (the complete document title as indicated on the title page. Its classification should be indicated by the appropriate abbreviation (S,C,R or U) in parentheses after the title.)

Numerical Simulation of Flows Near and Through a Two-Dimensional Array of Buildings (U)

4. AUTHORS (Last name, first name, middle initial. If military, show rank, e.g. Doe, Maj. John E.)

Yee, Eugene, Lien, F.S, and Cheng, Y.

5. DATE OF PUBLICATION (month and year of publication of document)

December 2001

6a. NO. OF PAGES (total containing information. Include Annexes, Appendices, etc.)

54

6b. NO. OF REFS (total cited in document)

12

6. DESCRIPTIVE NOTES (the category of the document, e.g. technical report, technical note or memorandum. If appropriate, enter the type of report, e.g. interim, progress, summary, annual or final. Give the inclusive dates when a specific reporting period is covered.)

Technical Report (Final) [1 May, 2001 to 30 November, 2001]

8. SPONSORING ACTIVITY (the name of the department project office or laboratory sponsoring the research and development. Include the address.)

Defence Research Establishment Suffield
P.O. Box 4000
Medicine Hat, Alberta T1A 8K6

9a. PROJECT OR GRANT NO. (if appropriate, the applicable research and development project or grant number under which the document was written. Please specify whether project or grant)

PCN No. 6QD11

9b. CONTRACT NO. (if appropriate, the applicable number under which the document was written)

10a. ORIGINATOR'S DOCUMENT NUMBER (the official document number by which the document is identified by the originating activity. This number must be unique to this document.)

DRES TR 2001-115

10b. OTHER DOCUMENT NOS. (Any other numbers which may be assigned this document either by the originator or by the sponsor)

11. DOCUMENT AVAILABILITY (any limitations on further dissemination of the document, other than those imposed by security classification)

(X) Unlimited distribution
( ) Distribution limited to defence departments and defence contractors; further distribution only as approved
( ) Distribution limited to defence departments and Canadian defence contractors; further distribution only as approved
( ) Distribution limited to government departments and agencies; further distribution only as approved
( ) Distribution limited to defence departments; further distribution only as approved
( ) Other (please specify):

12. DOCUMENT ANNOUNCEMENT (any limitation to the bibliographic announcement of this document. This will normally correspond to the Document Availabilty (11). However, where further distribution (beyond the audience specified in 11) is possible, a wider announcement audience may be selected.)

No

13. ABSTRACT (a brief and factual summary of the document. It may also appear elsewhere in the body of the document itself. It is highly desirable that the abstract of classified documents be unclassified. Each paragraph of the abstract shall begin with an indication of the security classification of the information in the paragraph (unless the document itself is unclassified) represented as (S), (C), (R), or (U). It is not necessary to include here abstracts in both offical languages unless the text is bilingual).

A numerical simulation has been performed of turbulent flow near and through a two-dimensional array of rectangular buildings (bluff bodies) in a neutrally stratified background flow. The model used for the simulation was the steady-state Reynolds-averaged Navier-Stokes equations with an isotropic, linear eddy viscosity formulation for the Reynolds stresses; and, the eddy viscosity was determined using a high-Reynolds number form of the k-ε turbulence-closure model with the boundary conditions at the wall obtained with the wall-function approach. The resulting system of partial differential equations along with the concomitant boundary conditions for the problem was solved using the SIMPLE algorithm in conjunction with a non-orthogonal, colocated, cell-centered, finite volume procedure. The predictive capabilities of the numerical simulation of urban flow are validated against a very detailed and comprehensive wind tunnel data set. Vertical profiles of the mean streamwise and vertical velocities and the turbulence kinetic energy are presented and compared to those measured in the wind tunnel simulation. In addition to the comparison between modeled and measured results, the numerical simulation is used to aid in the interpretation of certain features of the flow observed in the wind tunnel simulation. It is found that the overall performance of the model is good---most of the qualitative features in the disturbed turbulent flow field in and near the building array are correctly reproduced, and the quantitative agreement is also generally fairly good (especially for the mean velocity field). The underestimation of the turbulence energy levels may arise from the inability of the model to capture the subtle effects of secondary strain, especially those associated with curvature, on the turbulence.

14. KEYWORDS, DESCRIPTORS or IDENTIFIERS (technically meaningful terms or short phrases that characterize a document and could be helpful in cataloguing the document. They should be selected so that no security classification is required. Identifiers, such as equipment model designation, trade name, military project code name, geographic location may also be included. If possible keywords should be selected from a published thesaurus. e.g. Thesaurus of Engineering and Scientific Terms (TEST) and that thesaurus-identified. If it is not possible to select indexing terms which are Unclassified, the classification of each should be indicated as with the title.)

Urban Flow Modeling
Building Arrays
Computational Fluid Dynamics
Model Validation

Defence R&D Canada
is the national authority for providing
Science and Technology (S&T) leadership
in the advancement and maintenance
of Canada's defence capabilities.

R et D pour la défense Canada
est responsable, au niveau national, pour
les sciences et la technologie (S et T)
au service de l'avancement et du maintien des
capacités de défense du Canada.

www.drdc-rddc.dnd.ca